Inorg. Chem. **2007**, *46*, 8533–8547

The Role of Substituents on Functionalized 1,10-Phenanthroline in Controlling the Emission Properties of Cationic Iridium(III) Complexes of Interest for Electroluminescent Devices

Claudia Dragonetti,[†,§,⊥] Luigi Falciola,[‡,§] Patrizia Mussini,*[,‡,§] Stefania Righetto,[†,§,⊥] Dominique Roberto,*[,†,§,||,⊥] Renato Ugo,[†,§,||,⊥] and Adriana Valore[†,§,⊥]

Dipartimento di Chimica Inorganica, Metallorganica e Analitica, Dipartimento di Chimica Fisica ed Elettrochimica, Centro di Eccellenza CIMAINA dell'Università di Milano, Istituto di Scienze e Tecnologie Molecolari, CNR, and UdR dell'INSTM di Milano, via Venezian 21, 20133 Milano, Italy

Filippo De Angelis, Simona Fantacci,* and Antonio Sgamellotti

Istituto di Scienze e Tecnologie Molecolari, CNR, c/o Dipartimento di Chimica, Università di Perugia, via Elce di Sotto 8, I-06123 Perugia, Italy

Miguel Ramon and Michele Muccini

Istituto per lo Studio dei Materiali Nanostrutturati, CNR, via P. Gobetti 101, I-40129 Bologna, Italy

Received March 3, 2007

The photophysical and electrochemical properties of the novel complexes $[Ir(ppy)_2(5\text{-}X\text{-}1,10\text{-}phen)][PF_6]$ (ppy = 2-phenylpyridine, phen = phenanthroline, X = NMe_2, NO_2), $[Ir(pq)_2(5\text{-}X\text{-}1,10\text{-}phen)][PF_6]$ (pq = 2-phenylquinoline, X = H, Me, NMe_2, NO_2), $[Ir(ppy)_2(4\text{-}Me,7\text{-}Me\text{-}1,10\text{-}phen)][PF_6]$, $[Ir(ppy)_2(5\text{-}Me,6\text{-}Me\text{-}1,10\text{-}phen)][PF_6]$, $[Ir(ppy)_2(2\text{-}Me,9\text{-}Me\text{-}1,10\text{-}phen)][PF_6]$, and $[Ir(pq)_2(4\text{-}Ph,7\text{-}Ph\text{-}1,10\text{-}phen)][PF_6]$ have been investigated and compared with those of the known reference complexes $[Ir(ppy)_2(4\text{-}Me \text{ or } 5\text{-}H \text{ or } 5\text{-}Me\text{-}1,10\text{-}phen)][PF_6]$ and $[Ir(ppy)_2(4\text{-}Ph,7\text{-}Ph\text{-}1,10\text{-}phen)][PF_6]$, showing how the nature and number of the phenanthroline substituents tune the color of the emission, its quantum yield, and the emission lifetime. It turns out that the quantum yield is strongly dependent on the nonradiative decay. The geometry, ground state, electronic structure, and excited electronic states of the investigated complexes have been calculated on the basis of density functional theory (DFT) and time-dependent DFT approaches, thus substantiating the electrochemical measurements and providing insight into the electronic origin of the absorption spectra and of the lowest excited states involved in the light emission process. These results provide useful guidelines for further tailoring of the photophysical properties of ionic Ir(III) complexes.

Introduction

Recently, many *neutral* heavy-transition-metal complexes have emerged as promising phosphorescent emitters for organic light-emitting diodes (OLED) with improved efficiency. These complexes are able to harvest both triplet and singlet excitons due to increased spin−orbit coupling, which in turn increases the efficiency of intercrossing into the emitting triplet state.[1] Neutral iridium(III) cyclometalated complexes are of particular interest because (i) they typically exhibit high phosphorescence quantum yields ($\phi = 10-90\%$) and (ii) their emission spectrum can be effectively tuned over

* To whom correspondence should be addressed. E-mail: simona@thch.unipg.it (S.F.), patrizia.mussini@unimi.it (P.M.), dominique.roberto@unimi.it (D.R.).
† Dipartimento di Chimica Inorganica, Metallorganica e Analitica.
‡ Dipartimento di Chimica Fisica ed Elettrochimica.
§ Centro di Eccellenza CIMAINA dell'Università di Milano.
|| Istituto di Scienze e Tecnologie Molecolari, CNR.
⊥ UdR dell'INSTM di Milano.

(1) Evans, R. C.; Douglas, P.; Winscom, C. J. *Coord. Chem. Rev.* **2006**, *250*, 2093.

10.1021/ic700414z CCC: $37.00
Published on Web 09/21/2007

a large spectral range by an appropriate choice and combination of ligands and ligand substituents.[1,2] These characteristics suggested their use as emitting materials in host−guest architectures typically employed in OLED devices.[1,3] A recent concept in solid-state electroluminescence proposes the use of "*ionic* transition-metal complexes" (iTMCs)[4] thin films as active layers in electroluminescent devices. Unlike neutral metal complexes, iTMCs contain mobile counterions that facilitate charge transport across the film and eliminate the need for electron- and hole-injection layers. The iTMC-based *single-layer* electroluminescent devices may also operate at low voltage with high workfunction air-stable electrodes (e.g., gold), due to the high electric fields produced by ions accumulating at the anode and cathode interfaces, which favor charge injection.[4] The first reports on single-layer devices involving ionic transition-metal complexes were based on ruthenium(II) (e.g., $[Ru(2,2'\text{-bipyridine})_3]^{2+}$),[5] osmium(II),[6] and Re(I)[7] complexes, characterized primarily by an orange-red emission and by a limited possibility of tuning the emission wavelength. It was only 3 years ago that an ionic cyclometalated iridium(III) complex, $[Ir(ppy)_2(4,4'\text{-di-}tert\text{-butyl-}2,2'\text{-bipyridine})][PF_6]$ (ppy = cyclometalated 2-phenylpyridine), was first used in electroluminescent devices affording yellow emission.[8] Since then, ionic iridium(III) complexes have attracted wide interest mainly due to the possibility of inducing broad emission color tuning by changing the ligand.[4,8−15]

Almost all investigated ionic iridium complexes contain two cyclometalated 2-phenylpyridines and one bipyridine. The spectral tuning of the emission is accomplished by functionalizing the former[4,8,11] or the latter[9] ligand. In particular, it was reported that the emission color of complexes such as $[Ir(pic)_2(L)][PF_6]$ (pic = cyclometalated 1-phenylisoquinoline; L = bidentate nitrogen donor ligand such as 1,2-bipyridine, 1,10-phenanthroline, 2-pyridyl-quinoline, 2,2′-biquinoline, 1,1′-biisoquinoline, or 2-(2-quinolinyl)-quinoxaline)) can be significantly tuned by changing the nature of the ligand L.[13] Recently, a combinatorial approach highlighted the potential emission color tunability of $[Ir(ppy)_2(\text{substituted 1,10-phen})]^+$ (phen = phenanthroline) complexes by changing the nature and position of substituents.[10,12] Basically, the quantum yield of $[Ir(ppy)_2(1,10\text{-phen})]^+$ is reported to be 2 times higher than that of $[Ir(ppy)_2(2,2'\text{-bipyridine})]^+$, but phenanthrolines substituted with alkyl groups such as 3,4,7,8-tetramethyl-1,10-phenanthroline and 4- or 5-methyl-1,10-phenanthroline were predicted to lead to even higher quantum yields,[10] whereas a slightly lower quantum yield was predicted for the complex with 4,7-diphenyl-1,10-phenanthroline.[12] However, contrary to what was predicted by the combinatorial approach, for $[Ir(ppy)_2(4\text{-Ph,7-Ph-1,10-phen})][PF_6]$, a quantum yield 1.5 times higher than that of $[Ir(ppy)_2(1,10\text{-phen})][PF_6]$ was reported, suggesting that predictions need to be verified experimentally.[12] Finally, the potential application of these cationic Ir(III) complexes as electroluminescent materials was confirmed by the preparation of a stable *single-layer* light-emitting electrochemical cell using $[Ir(ppy)_2(4\text{-Ph,7-Ph-1,-10-phen})][PF_6]$.[15b]

These promising results prompted us to perform a systematic investigation of the photophysical and electrochemical properties of the new class of ionic Ir(III) complexes with substituted 1,10-phenanthrolines in order to experimentally assess the role of substituents located on various positions of the phenanthroline ligand. Thus, a large number of Ir(III) complexes was investigated (**1**−**7**, Figure 1).

The electronic origin of the experimental photophysical and electrochemical data was also substantiated by a density functional theory (DFT) investigation, with particular reference to the nature of the highest-occupied molecular orbital (HOMO) and lowest-unoccupied molecular orbital (LUMO)

(2) See, for example: (a) Nazeeruddin, M. K.; Humphrey-Baker, R.; Berner, D.; Rivier, S.; Zuppiroli, L.; Graetzel, M. *J. Am. Chem. Soc.* **2003**, *125*, 8790 and references therein. (b) Lepeltier, M.; Le Bozec, H.; Guerchais, V.; Lee, T. K.-M.; Lo, K. K.-W. *Organometallics* **2005**, *24*, 6069 and references therein. (c) Hwang, F.-M.; Chen, H. Y.; Chen, P.-S.; Liu, C.-S.; Chi, Y.; Shu, C. F.; Wu, F.-L.; Chou, P. T.; Peng, S.-M.; Lee, G.-H. *Inorg. Chem.* **2005**, *44*, 1344.

(3) See, for example: (a) Baldo, M. A.; Lamansky, S.; Burrows, P. E.; Thompson, M. E.; Forrest, S. R. *Appl. Phys. Lett.* **1999**, *75*, 4. (b) Adachi, C.; Baldo, M. A.; Forrest, S. R.; Lamansky, S.; Thompson, M. E.; Kwong, R. C. *Appl. Phys. Lett.* **2001**, *78*, 1622. (c) Adachi, C.; Kwong, R. C.; Djurovich, P.; Adamovich, V.; Baldo, M. A.; Thompson, M. E.; Forrest, S. R. *Appl. Phys. Lett.* **2001**, *79*, 2082. (d) Adachi, C.; Baldo, M. A.; Thompson, M. E.; Forrest, S. R. *J. Appl. Phys.* **2001**, *90*, 5048. (e) Lamansky, S.; Djurovich, P.; Murphy, D.; Abdel-Razzaq, F.; Lee, H.-E.; Adachi, C.; Burrows, P. E.; Forrest, S. R.; Thompson, M. E. *J. Am. Chem. Soc.* **2001**, *123*, 4304. (f) Xie, H. Z.; Liu, M. W.; Wang, O. Y.; Zhang, X. H.; Lee, C. S.; Hung, L. S.; Lee, S. T.; Teng, P. F.; Kwong, H. L.; Zhen, H.; Che, C. M. *Adv. Mater.* **2001**, *13*, 1245. (g) Duan, J.-P.; Sun, P.-P.; Cheng, C.-H. *Adv. Mater.* **2003**, *15*, 224. (h) Tsuzuki, T.; Shirasawa, N.; Suzuki, T.; Tokito, S. *Adv. Mater.* **2003**, *15*, 1455. (i) Laskar, I. R.; Chen, T.-M. *Chem. Mater.* **2004**, *16*, 111. (j) Laskar, I. R.; Hsu, S.-F.; Chen, T.-M. *Polyhedron* **2005**, *24*, 189. (k) Tokito, S.; Tsuzuki, T.; Sato, F.; Iijima, T. *Curr. Appl. Phys.* **2005**, 331.

(4) Lowry, M. S.; Goldsmith, J. I.; Slinker, J. D.; Rohl, R.; Pascal, R. A., Jr.; Malliaras G. G.; Bernhard, S. *Chem. Mater.* **2005**, *17*, 5712 and references therein.

(5) (a) Handy, E. S.; Pal, A. J.; Rubner, M. F. *J. Am. Chem. Soc.* **1999**, *121*, 3525. (b) Gao, F. G.; Bard, A. J. *J. Am. Chem. Soc.* **2000**, *122*, 7426.

(6) Bernhard, S.; Gao, X.; Abruna, H. D.; Malliaras, G. G. *Adv. Mater.* **2002**, *14*, 433.

(7) Gong, X.; Ng, P. K.; Chan, W. K. *Adv. Mater.* **1998**, *10*, 1337.

(8) Slinker, J. D.; Gorodetsky, A. A.; Lowry, M. S.; Wang, J.; Parker, S.; Rohl, R.; Bernhard, S.; Malliaras, G. G. *J. Am. Chem. Soc.* **2004**, *126*, 2763.

(9) (a) Neve, F.; La Deda, M.; Crespini, A.; Bellusci, A.; Puntoriero, F.; Campagna, S. *Organometallics* **2004**, *23*, 5856. (b) Lepeltier, M.; Lee, T. K.-M.; Lo, K. K.-W.; Toupet, L.; Le Bozec, H.; Guerchais, V. *Eur. J. Inorg. Chem.* **2005**, 110.

(10) Lowry, M. S.; Hudson, W. R.; Pascal, R. A., Jr.; Bernhard, S. *J. Am. Chem. Soc.* **2004**, *126*, 14129.

(11) Slinker, J. D.; Koh, C. Y.; Malliaras, G. G.; Lowry, M. S.; Bernhard, S. *Appl. Phys. Lett.* **2005**, *86*, 173506.

(12) Goldsmith, J. I.; Hudson, W. R.; Lowry, M. S.; Anderson, T. H.; Bernhard, S. *J. Am. Chem. Soc.* **2005**, *127*, 7502.

(13) Zhao, Q.; Liu, S.; Shi, M.; Wang, C.; Yu, M.; Li, L.; Li, F.; Yi, T.; Huang, C. *Inorg. Chem.* **2006**, *45*, 6152.

(14) Neve, F.; La Deda, M.; Puntoriero, F.; Campagna, S. *Inorg. Chim. Acta* **2006**, *359*, 1666.

(15) See, for example: (a) Nazeruddin, M. K.; Wehg, R. T.; Zhou, Z.; Klein, C.; Wang, Q.; De Angelis, F.; Fantacci, S.; Grätzel, M. *Inorg. Chem.* **2006**, *45*, 9245. (b) Bolink, H. J.; Cappelli, L.; Coronado, E.; Grätzel, M.; Ortì, E.; Costa, R. D.; Viruela, P. M.; Nazeeruddin, M. K. *J. Am. Chem. Soc.* **2006**, *128*, 14787. (c) Wilkinson, A. J.; Goeta, A. E.; Foster, C. E.; Williams, J. A. G. *Inorg. Chem.* **2004**, *43*, 6513. (d) De Angelis, F.; Fantacci, S.; Evans, N.; Klein, C.; Zakeeruddin, S. M.; Moser, J.-E.; Kalyanasundaram, K.; Bolink, H. J.; Grätzel, M.; Nazeeruddin, M. K. *Inorg. Chem.* **2007**, *46*, 5989.

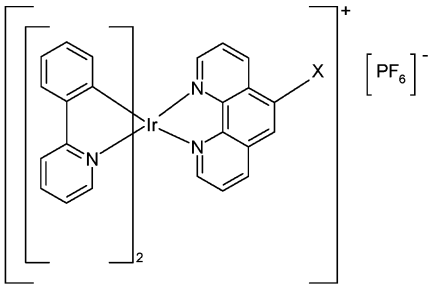

1 $[Ir(ppy)_2(5\text{-}X\text{-}1,10\text{-}phen)]^+$
- 1a X = Me
- 1b X = NMe_2
- 1c X = NO_2
- 1d X = H

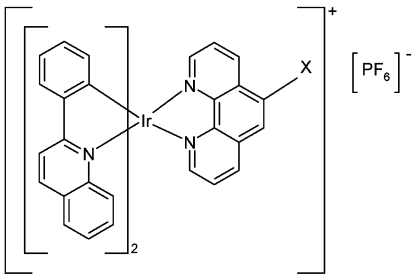

2 $[Ir(pq)_2(5\text{-}X\text{-}1,10\text{-}phen)]^+$
- 2a X = Me
- 2b X = NMe_2
- 2c X = NO_2
- 2d X = H

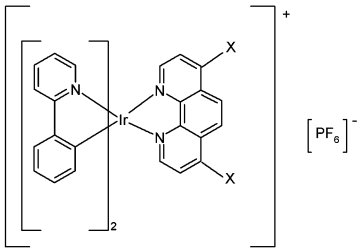

3 $[Ir(ppy)_2(4\text{-}X,7\text{-}X\text{-}1,10\text{-}phen)]^+$
- 3a X = Ph
- 3b X = Me

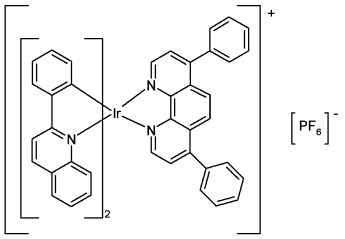

4 $[Ir(pq)_2(4\text{-}Ph,7\text{-}Ph\text{-}1,10\text{-}phen)]^+$

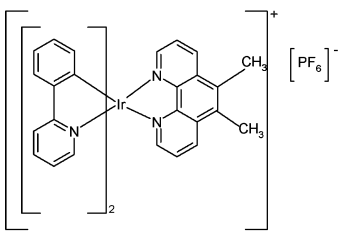

5 $[Ir(ppy)_2(5\text{-}Me,6\text{-}Me\text{-}1,10\text{-}phen)]^+$

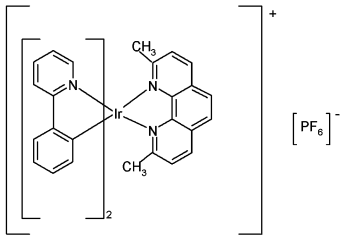

6 $[Ir(ppy)_2(2\text{-}Me,9\text{-}Me\text{-}1,10\text{-}phen)]^+$

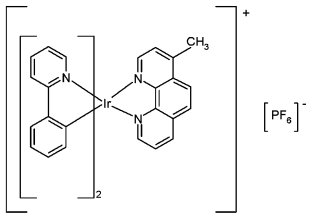

7 $[Ir(ppy)_2(4\text{-}Me\text{-}1,10\text{-}phen)]^+$

Figure 1. Complexes investigated corresponding to $[Ir(ppy)_2(substituted\text{-}1,10\text{-}phen)][PF_6]$ and $[Ir(pq)_2(substituted\text{-}1,10\text{-}phen)][PF_6]$ (ppy = 2-phenylpyridine and pq = 2-phenylquinoline, both cyclometalated).

states and also of the lowest excited states involved in the absorption and emission processes, by means of time-dependent DFT calculations (TDDFT). While ground-state DFT calculations have become increasingly popular together with experimental electrochemical measurements to define the nature of the redox processes involving iridium(III) compounds,[4,10,13,16] only a few TDDFT excited-state calculations on iridium(III) complexes have been reported to date,[17] a pioneering paper in the field being the work by Hay[17a] on the neutral $[Ir(ppy)_3]$ complex.

Experimental Section

General Comments. All reagents and solvents were purchased from Sigma-Aldrich, while $IrCl_3$ hydrate was purchased from Engelhard. The cyclometalated Ir(III) chloro-bridge dimers $[Ir(ppy)_2Cl]_2$ and $[Ir(pq)_2Cl]_2$ (pq= 2-phenylquinoline) were prepared according to the literature.[18] The 5-NMe_2-1,10-phen compound was synthesized as previously reported.[19] All reactions were carried out

(16) See, for example: (a) Tamayo, A. B.; Garon, S.; Sajoto, T.; Djurovich, P. I.; Tsyba, I. M.; Bau, R.; Thompson, M. E. *Inorg. Chem.* **2005**, *44*, 8723. (b) You, Y.; Park, S. Y. *J. Am. Chem. Soc.* **2005**, *127*, 12438. (c) Lo, S. C.; Shipley, C. P.; Bera, R. N.; Harding, R. E.; Cowley, A. R.; Burn, P. L.; Samuel, I. D. W. *Chem. Mater.* **2006**, *18*, 5119. (d) Dedeian, K.; Shi, J.; Shepherd, N.; Forsythe, E.; Morton, D. C. *Inorg. Chem.* **2005**, *44*, 4445.

(17) See, for example: (a) Hay, P. J. *J. Phys. Chem. A* **2002**, *106*, 1634. (b) Yang, C.-H.; Li, S.-W.; Chi, Y.; Cheng, Y.-M.; Yeh., Y.-S.; Chou, P.-T.; Lee, G.-H.; Wang, C. H.; Shu, C. F. *Inorg. Chem.* **2005**, *44*, 7770. (c) Polson, M.; Ravaglia, M.; Fracasso, S.; Garavelli, M.; Scandola, F. *Inorg. Chem.* **2005**, *44*, 1282. (d) Yang, C. H.; Su, W. L.; Fang, K. H.; Wang, S. P.; Sun, I. W. *Organometallics* **2006**, *25*, 4514. (e) Polson, M.; Fracasso, S.; Bertolasi, V.; Ravaglia, M.; Scandola, F. *Inorg. Chem.* **2004**, *43*, 1950. (f) Obara, S.; Itabashi, M.; Okuda, F.; Tamaki, S.; Tanabe, Y.; Ishii, Y.; Nozaki, K.; Haga, M.-A. *Inorg. Chem.* **2006**, *45*, 8907.

(18) Sprouse, S.; King, K. A.; Spellane, P. J.; Watts, R. J. *J. Am. Chem. Soc.* **1984**, *106*, 6647.

(19) Shan, Y.; Sullivan, B. P. *Inorg. Chem.* **1995**, *34*, 6235.

under nitrogen. ^{1}H NMR spectra were obtained on a Bruker Avance 400 MHz instrument. Elemental analyses were carried out in the Dipartimento di Chimica Inorganica, Metallorganica e Analitica of Milan University.

Synthesis of Complexes. All $[Ir(ppy)_2L][PF_6]$ and $[Ir(pq)_2L][PF_6]$ (L = 1,10-phen) complexes were prepared with the same procedure, described below in the case of **1a**, slightly modified with respect to the literature.[9,13] Complexes **1d** and **3a** were previously prepared and isolated;[10,12] **1a** was previously obtained by a combinatorial approach[10] but never isolated whereas all the other complexes (**1b, 1c**, **2a**, **2b**−**2d**, **3b**, and **4**−**6**) are new, to our knowledge.

$[Ir(ppy)_2$(5-Me-1,10-phen)$][PF_6]$ (1a). A solution of $[Ir(ppy)_2Cl]_2$ (0.083 g, 0.077 mmol) and 5-Me-1,10-phen (0.030 g, 0.154 mmol) in CH_2Cl_2−MeOH (15 mL, 2:1 v/v) was heated under reflux. After 5−6 h, the orange solution was cooled to room temperature, and then a 10-fold excess of ammonium hexafluorophosphate was added. The suspension was stirred for 15 min and then filtered to remove insoluble inorganic salts. The solution was evaporated to dryness under reduced pressure to obtain a crude orange solid. The solid was dissolved in CH_2Cl_2 and filtered to remove the residual traces of inorganic salts. Diethyl ether was layered onto the orange filtrate, and the mixture was cooled to ∼0 °C. Orange plates of the desired product formed overnight. Yield: 0.093 g (72%). ^{1}H NMR (400 MHz, CD_2Cl_2) δ: 8.74 (d, J = 8.46 Hz, 1H), 8.55 (d, J = 8.26 Hz, 1H), 8.38 (d, J = 5.01 Hz, 1H), 8.31 (d, J = 5.03 Hz, 1H), 8.04 (s, 1H), 8.00 (d, J = 8.30 Hz, 2H), 7.83 (m, 6H), 7.35 (t, J = 5.36 Hz, 2H), 7.16 (t, J = 7.56 Hz, 2H), 7.03 (t, J = 8.08 Hz, 2H), 6.88 (t, J = 6.63 Hz, 2H), 6.46 (d, J = 7.16 Hz, 2H), 2.95 (s, 3H). Anal. Calcd for Ir $C_{35}H_{26}N_4PF_6$: C, 50.06; H, 3.12; N, 6.67. Found: C, 49.89; H, 3.08; N, 6.78.

$[Ir(ppy)_2$(5-NMe$_2$-1,10-phen)$][PF_6]$ (1b). Yield: 0.082 g (61%, starting from 0.0825 g, 0.077 mmol of $[Ir(ppy)_2Cl]_2$). ^{1}H NMR (400 MHz, CD_2Cl_2) δ: 8.86 (d, J = 8.52 Hz, 1H), 8.44 (d, J = 8.18 Hz, 1H), 8.34 (d, J = 3.49 Hz, 1H), 8.14 (d, J = 3.39 Hz, 1H), 7.99 (d, J = 8.00 Hz, 1H), 7.76 (m, 6H), 7.59 (m, 1H), 7.52 (s, 1H), 7.38 (s, 2H), 7.15 (t, J = 7.37 Hz, 2H), 7.02 (d, J = 6.44 Hz, 2H), 6.89 (t, J = 6.38 Hz, 2H), 6.44 (t, J = 8.35 Hz, 2H), 3.11(s, 6H). Anal. Calcd for Ir $C_{36}H_{29}N_5PF_6$: C, 49.77; H, 3.36; N, 8.06. Found: C, 49.69; H, 3.28; N, 7.98.

$[Ir(ppy)_2$(5-nitro-1,10-phen)$][PF_6]$ (1c). Yield: 0.058 g (87%, starting from 0.0410 g, 0.0383 mmol of $[Ir(ppy)_2Cl]_2$). ^{1}H NMR (400 MHz, CD_2Cl_2) δ: 9.32 (d, J = 8.74 Hz, 1H), 9.16 (s, 1H), 8.89 (d, J = 8.18 Hz, 1H), 8.56 (d, J = 4.49 Hz, 1H), 8.52 (d, J = 4.99 Hz, 1H), 8.02 (m, 4H), 7.80 (m, 4H), 7.38 (t, J = 4.51 Hz, 2 H), 7.17 (t, J = 7.48 Hz, 2H), 7.05 (t, J = 7.40 Hz, 2H), 6.93 (t, J = 7.06 Hz, 2H), 6.44 (d, J = 7.51 Hz, 2H) Anal. Calcd for Ir $C_{34}H_{23}N_5O_2PF_6$: C, 46.90; H, 2.66; N, 8.04. Found: C, 46.92; H, 2.70; N, 8.10.

$[Ir(ppy)_2$(1,10-phen)$][PF_6]$ (1d). Yield: 0.103 g (80%, starting from 0.0489 g, 0.0385 mmol of $[Ir(ppy)_2Cl]_2$). ^{1}H NMR (400 MHz, CD_2Cl_2) δ: 8.66 (d, J = 8.00 Hz, 2H), 8.38 (d, J = 4.00 Hz, 2H), 8.24 (s, 2H), 8.00 (d, J = 8.00 Hz, 2H), 7.83 (m, 6H), 7.35 (d, J = 5.2 Hz, 2H), 7.16 (t, J = 7.3 Hz, 2H), 7.04 (t, J = 7.3 Hz, 2H), 6.88 (t, J = 5.8 Hz, 2H), 6.46 (d, J = 6.6 Hz, 2H). Anal. Calcd for Ir $C_{34}H_{24}N_4PF_6$: C, 49.46; H, 2.93; N, 6.78. Found: C, 49.38; H, 2.88; N, 6.72.

$[Ir(pq)_2$ 5-Me-1,10-phen$)][PF_6]$ (2a). Yield: 0.0772 g (67%, starting from 0.0780 g, 0.0613 mmol of $[Ir(pq)_2Cl]_2$). ^{1}H NMR (400 MHz, CD_2Cl_2) δ: 8.62 (d, J = 5.05 Hz, 1H), 8.55 (m, 2H), 8.37 (d, J = 8.26 Hz, 1H), 8.24 (m, 4H), 8.17 (d, J = 7.4 Hz, 2H), 7.87 (d, J = 8.41 Hz, 1H), 7.80 (d, J = 8.19 Hz, 1H), 7.72 (s, 1 H), 7.67 (d, J = 8.06 Hz, 2H), 7.25 (m, 6H), 6.91 (t, J = 7.20 Hz, 2H), 6.81 (t, J = 7.94 Hz, 2H), 6.7 (m, 2H), 2.72 (s, 3H). Anal. Calcd for Ir $C_{43}H_{30}N_4PF_6$: C, 54.95; H, 3.22; N, 5.96. Found: C, 54,78; H, 3.16; N, 6.00.

$[Ir(pq)_2$(5-NMe$_2$-1,10-phen)$][PF_6]$ (2b). Yield: 0.0731 g (60%, starting from 0.080 g, 0.0629 mmol of $[Ir(pq)_2Cl]_2$). ^{1}H NMR (400 MHz, CD_2Cl_2) δ: 8.72 (d, J = 8.5 Hz, 1H), 8.58 (d, J = 4.5 Hz, 1H), 8.39 (d, J = 4.80 Hz, 1H), 8.27 (m, 5H), 8.16 (dd, J = 10.65 Hz, 2H), 7.82 (dd, J = 8.45 Hz, 1H), 7.69 (m, 3 H), 7.27 (m, 6H), 7.18 (d, J = 8.95 Hz, 1H), 6.87 (m, 4H), 6.69 (dd, J = 18 Hz, 2H), 2.92 (s, 2H). Anal. Calcd for Ir $C_{44}H_{33}N_5PF_6$: C, 54.54; H, 3.43; N, 7.23. Found: C, 54.46; H, 3.35; N, 7.12.

$[Ir(pq)_2$(5-nitro-1,10-phen)$][PF_6]$ (2c). Yield: 0.060 g (80%, starting from 0.0491 g, 0.0386 mmol of $[Ir(pq)_2Cl]_2$). ^{1}H NMR (400 MHz, CD_2Cl_2) δ: 9.16 (d, J = 8.72 Hz, 1H), 8.83 (s, 1H), 8.78 (d, J = 5.08 Hz, 1H), 8.71 (d, J = 8.20 Hz, 1H), 8.29 (m, 4H), 8.19 (d, J = 7.88 Hz, 2H), 8,02 (m, 2H), 7.69 (d, J = 8.09 Hz, 2 H), 7.28 (m, 4H), 7.14 (m, 2H), 6.93 (t, J = 7.48 Hz, 2H), 6.85 (t, J = 8.58 Hz, 2H), 6.70 (d, J = 7.25 Hz, 2H). Anal. Calcd for Ir $C_{42}H_{27}N_5O_2PF_6$: C, 51.96; H, 2.80; N, 7.21. Found: C, 51.78; H, 2.78; N, 7.16.

$[Ir(pq)_2$(1,10-phen)$][PF_6]$ (2d). Yield: 0.077 g (68%, starting from 0.080 g, 0.0629 mmol of $[Ir(pq)_2Cl]_2$). ^{1}H NMR (400 MHz, CD_2Cl_2) δ: 8.61 (dd, J = 5.14 Hz, 1H), 8.47 (dd, J = 8.20 Hz, 1H), 8.26 (q, J = 8.82, 2H), 8.16 (d, J = 7.07 Hz, 1H), 7.92 (s, 1H), 7.84 (dd, J = 8.20 Hz, 1H), 7.66 (dd, J = 8.06 Hz, 1H), 7.26 (m, 3H), 6.92 (t, J = 7.59 Hz, 1H), 6.79 (t, J = 6.94 Hz, 1H), 6.71 (dd, J = 7.66 Hz, 1H). Anal. Calcd for Ir$C_{42}H_{28}N_4PF_6$: C, 54.49; H, 3.05; N, 6.05. Found: C, 54.56; H, 3.10; N, 5.96.

$[Ir(ppy)_2$(4-Ph,7-Ph-1,10-phen)$][PF_6]$ (3a). Yield: 0.081 g (61%, starting from 0.0728 g, 0.0689 mmol of $[Ir(ppy)_2Cl]_2$). ^{1}H NMR (400 MHz, CD_2Cl_2) δ: 8.43 (d, J = 5.26 Hz, 2H), 8.23 (s, 2H), 8.04 (d, J = 8.12 Hz, 2H), 7.85 (m, 4H), 7.78 (d, J = 5.27 Hz, 2H), 7.63 (m, 10H), 7,54 (d, J = 5.24 Hz, 2H), 7.16 (t, J = 7.65 Hz, 2 H), 7.06 (t, J = 7.50 Hz, 2H), 6.97 (t, J = 7.70 Hz, 2H), 6.50 (d, J = 6.91 Hz, 2H). Anal. Calcd for Ir $C_{46}H_{32}N_4PF_6$: C, 56.49; H, 3.29; N, 5.73. Found: C, 56.38; H, 3.28; N, 5.68.

$[Ir(ppy)_2$(4-Me,7-Me-1,10-phen)$][PF_6]$ (3b). Yield: 0.071 g (64%, starting from 0.0696 g, 0.0649 mmol of $[Ir(ppy)_2Cl]_2$). ^{1}H NMR (400 MHz, CD_2Cl_2) δ: 8.37 (s, 2H), 8.22 (d, J = 5.00 Hz, 2H), 7.99 (d, J = 5.00 Hz, 2H), 7.81 (d, J = 10.00 Hz, 2H), 7.76 (t, J = 7.5 Hz, 2H), 7.64 (d, J = 5.00 Hz, 2H), 7.37 (d, J = 5.0 Hz, 2H), 7.15 (t, J = 7.5 Hz, 2H), 7.02 (t, J = 5 Hz, 2H), 6.88 (t, J = 5.8 Hz, 2H), 6.45 (d, J = 6.6 Hz, 2H), 2.99 (s, 6H). Anal. Calcd for Ir $C_{36}H_{28}N_4PF_6$: C, 50.64; H, 3.30; N, 6.56. Found: C, 50.70; H, 3.26; N, 6.60.

$[Ir(pq)_2$(4-Ph,7-Ph-1,10-phen)$][PF_6]$ (4). Yield: 0.070 g (60% starting from 0.0689 g, 0.0541 mmol of $[Ir(pq)_2Cl]_2$). ^{1}H NMR (400 MHz, CD_2Cl_2) δ: 8.72 (d, J = 5.37 Hz, 2H), 8.31 (m, 4H), 8.19 (d, J = 7.87 Hz, 2H), 7.93 (s, 2H), 7.79 (d, J = 5.38 Hz, 2H), 7.72 (d, J = 7.16 Hz, 2H), 7.59 (m, 6H), 7.48 (m, 4H), 7.32 (m, 6H), 6.91 (m, 4H), 6.72 (d, J = 7.65 Hz, 2H). Anal. Calcd for Ir $C_{54}H_{36}N_4PF_6$: C, 60.16; H, 3.34; N, 5.20. Found: C, 60.18; H, 3.38; N, 5.30.

$[Ir(ppy)_2$(5-Me,6-Me-1,10-phen)$][PF_6]$ (5). Yield: 0.060 g (65%, starting from 0.0579 g, 0.0541 mmol of $[Ir(ppy)_2Cl]_2$). ^{1}H NMR (400 MHz, CD_2Cl_2) δ: 8.78 (d, J = 5.00 Hz, 2H), 8.32 (d, J = 5.00 Hz, 2H), 8.00 (d, J = 10.00 Hz, 2H), 7.81 (m, 6H), 7.34 (d, J = 5.0 Hz, 2H), 7.16 (t, J = 7.5 Hz, 2H), 7.03 (t, J = 7.5 Hz, 2H), 6.87 (t, J = 8.33 Hz, 2H), 6.46 (d, J = 5.0 Hz, 2H), 5.36 (d, J = 5.0 Hz, 2H), 2.90 (s, 6H). Anal. Calcd for Ir $C_{36}H_{28}N_4PF_6$: C, 50.64; H, 3.30; N, 6.56. Found: C, 50.70; H, 3.26; N, 6.68.

$[Ir(ppy)_2$(2-Me,9-Me-1,10-phen)$][PF_6]$ (6). Yield: 0.110 g (83%, starting from 0.0832 g, 0.0776 mmol of $[Ir(ppy)_2Cl]_2$). ^{1}H

Table 1. Photophysical Data Obtained in CH_2Cl_2 Solution of Complexes **1**−**6**: Absorption and Emission Maxima, Quantum Yield (Φ), Lifetime (τ), Radiative Rate Constant (k_r), and Nonradiative Rate Constant (k_{nr})

	absorption maxima (nm) [ϵ (M^{-1} cm^{-1})]	emission maxima (nm; eV)	Φ[a] (%)	τ[b] (μs)	k_r (10^5 s^{-1})	k_{nr} (10^5 s^{-1})
1a	255 (sh), 268 [60300] 333 (sh), 377 [8070] 410 (sh)	559; 2.218	38	3.17	1.20	1.96
1b	252 (sh), 264 [81400] 334 (sh)	568; 2.183	0.3	n.d.	n.d.	n.d.
1c	254 (sh), 264 [86900] 378 [12400]		<0.1	n.d.	n.d.	n.d.
1d	252 (sh), 264 [58500] 377 [9130]	575; 2.156	7	1.31	0.53	7.10
2a	273 [70400] 329 [20700], 347 (sh) 431 [4750]	556; 2.230	34	4.03	0.84	1.64
2b	260 [97000] 332 [44100], 349 (sh) 434 [10900]	557; 2.226	6	n.d.	n.d.	n.d.
2c	268 [81100] 324 [27600] 430 [6930]		<0.1	n.d.	n.d.	n.d.
2d	269 [95000] 330 [41300] 433 [14700]	552; 2.246	6	n.d.	n.d.	n.d.
3a	269 [51300], 282 (sh) 385 [9020]	592; 2.094	20[c]	1.31	1.53	6.11
3b	255 (sh), 265 [73000] 375 (sh)	552; 2.246	26	1.43	1.82	5.17
4	267 (sh), 282 [80800] 329 [34400], 389 (sh) 433 [6060]	562; 2.206	19	2.39	0.79	3.39
5	242 [61800], 250 (sh) 269 [58200] 377 [8940]	568; 2.183	22	1.27	1.73	6.14
6	252 (sh), 269 [106000] 372 (sh)	534; 2.322	19	2.31	0.82	3.51

[a] By using coumarin 540 (Φ is 56% in EtOH; λ_{max} emission = 540 nm) as the reference;[21a] it is worth pointing out that lower quantum yields were obtained by working in CH_3CN or toluene instead of CH_2Cl_2 solution: Φ in CH_3CN is 7.7, 8, 4, and 5.7% for **1a**, **2a**, **3a**, and **4**, respectively; Φ in toluene is 2.7% for **3a**. [b] Values of τ significantly decrease (**1a**, 0.69; **1d**, 0.19; **2a**, 0.82; **3a**, 0.33; **3b**, 0.19; **4**, 0.67; **5**, 0.25; **6**, 0.26) when working with non-deaerated solutions, probably due to oxygen-triplet state interaction. [c] For this complex, various quantum yields were reported (Φ in CH_3CN = 18.18%, using $[Ir(ppy)_2(bpy)]PF_6$ as the standard);[12] Φ in CH_3CN = 53%, using $[Ru(4,7\text{-diphenyl-}1,10\text{-phen})_3]Cl_2$ as the standard;[15b] for the same cationic Ir complex but with Cl^- instead of PF_6^- as the counterion, Φ in CH_3CN = 10.25%, obtained by a combinatorial method and using $[Ir(ppy)_2(bpy)]Cl$ as the standard[12]).

NMR (400 MHz, CD_2Cl_2) δ: 8.51 (d, J = 10.00 Hz, 2H), 8.08 (s, 2H), 8.00 (d, J = 10.00 Hz, 2H), 7.81 (t, J = 7.5 Hz, 2H), 7.72 (d, J = 10.0 Hz, 2H), 7.65 (d, J = 10 Hz, 2H), 7.49 (d, J = 5 Hz, 2H), 7.03 (t, J = 7.5 Hz, 2H), 6.91 (t, J = 6.67 Hz, 2H), 6.85 (t, J = 7.5 Hz, 2H), 6.20 (d, J = 10.0 Hz, 2H), 2.19 (s, 6H). Anal. Calcd for Ir $C_{36}H_{28}N_4PF_6$: C, 50.64; H, 3.30; N, 6.56. Found: C, 50.70; H, 3.31; N, 6.70.

Photophysical Measurements. UV spectra were recorded at room temperature in a 1 cm quartz cuvette using a Jasco V-570 spectrometer. Emission spectra were recorded using a Jobin-Yvon Fluorolog-3 spectrometer equipped with double monochromators and a Hamamatsu-928 photomultiplier tube as the detector. All complexes were excited at 260 nm. Emission quantum yields have been determined, using the method of Demas and Crosby,[20] by comparison with the emission of coumarin 540, employed as a standard.[21a] The use of coumarin 540 as a reference standard seems more suitable than the use of $[Ru(bpy)_3]Cl_2$,[21b] which is very air sensitive. All solutions were deaerated by nitrogen bubbling for 30 min before measurements.

Lifetimes of the electronic emitting states were measured by exciting photoluminescence of CH_2Cl_2 solutions by the third harmonic (355 nm) of a Nd:YAG laser with a 25 ns pulse duration and a 20 Hz repetition rate. The photoluminescence was detected by a fast photomultiplier and then fed into a fast digital oscilloscope for synchronous time-resolved data acquisition. The time resolution of the setup is about 50 ns, well below all measured lifetimes. All solutions were in a 10^{-5} M concentration range and were deaerated by argon bubbling for 10 min before measurement. Lifetimes significantly decrease (values in the range 0.19−0.82 μs) in solutions that were not deaerated, probably due to oxygen-triplet state interaction (see note in Table 1).

Electrochemical Measurements. The cyclovoltammetric (CV) measurements were carried out using an Autolab PGSTAT 30 potentiostat/galvanostat (EcoChemie, The Netherlands) run by a PC with GPES software, at scan rates in the range of 0.02−2 V s^{-1}, working in acetonitrile (CH_3CN, Merck, HPLC grade), with 0.1 M tetrabutylammonium hexafluorophosphate $[NBu_4]PF_6$ (Fluka, puriss electrochemical grade) as the supporting electrolyte. The ohmic drop was corrected by means of the positive feedback technique.[22] A glassy-carbon (GC) electrode (Amel, surface area = 0.071 cm^2) was used as the working electrode, a platinum wire was used as the counter electrode, and an aqueous saturated calomel electrode (SCE) was used as the operating reference electrode. The

(20) Demas, J. N.; Crosby, G. A. *J. Phys. Chem.* **1971**, *75*, 991.
(21) (a) Kubin, R. F.; Fletcher, A. N. *Chem. Phys. Lett.* **1983**, *99*, 49. (b) Caspar, J. V.; Meyer, T. J. *J. Am. Chem. Soc.* **1983**, *105*, 5583.
(22) Bard, A. J.; Faulkner, L.R. *Electrochemical Methods. Fundamentals and Applications*; Wiley: New York, 2002; pp 648−650.

data have been subsequently referred to the $Me_{10}Fc^+|Me_{10}Fc$ (decamethylferricinium|decamethylferrocene) reference redox couple, currently proposed as an improved alternative[23−25] to ferrocene, recommended by IUPAC,[26,27] and whose formal redox potential in our operative solvent is −0.110 V against our aqueous SCE reference. The cell was thermostated at 298 K, and the solutions were carefully deaerated by nitrogen bubbling before the scans. The optimized polishing procedure for the working GC electrode consisted of surface treatment with diamond powder (Aldrich, diameter = 1 μm) on a wet cloth (DP-Nap, Struers). The chemical and electrochemical reversibility of each CV peak were checked by means of classical tests,[28] including analyses of: (a) half-peak width ($E_p - E_{p/2}$); (b) E_p vs log υ characteristics; (c) the distance between the forward and backward peak potential ($E_{p,f} - E_{p,b}$), and (d) the "stationary" steplike waves obtained by means of convolution analysis of the original CV characteristics,[29] for the evaluation of the half-wave potentials ($E_{1/2}$).

Computational Details. The geometries of all complexes were optimized by DFT calculations using the BP86 exchange-correlation function,[30,31] together with a TZP (DZP) basis set for Ir (N, C, O, H), including scalar-relativistic corrections as implemented in the *ADF* program.[32] The symmetric complexes **1d**, **3a**, **3b**, **4**, **5**, and **6** were optimized within C_2 symmetry constraints, while no symmetry constraints were considered for all the others. For complexes **1a**, **1d**, **2a**, **3a**, **3b**, and **4** we optimized the geometry of the lowest excited state by means of self-consistent field calculations imposing a triplet spin multiplicity.

On the ground-state-optimized geometries we performed single-point calculations at the B3LYP/LANL2DZ level of theory[33,34] in dichloromethane and acetonitrile solutions by means of the PCM solvation model,[35] as implemented in the *Gaussian 03* (G03) program package.[36] For complexes **1a**,**1d**, **3a**, and **3b** we performed TDDFT calculations at the B3LYP/LANL2DZ level of theory in dichloromethane solution. Calculation of the lowest 70 singlet−singlet excitations at the ground-state-optimized geometries allowed us to simulate a large (up to 250 nm) portion of the absorption spectrum. The simulation of the absorption spectra has been performed by a Gaussian convolution with fwhm = 0.4 eV; the experimental spectra have been rescaled so that the intensity of the experimental and theoretical main features in the absorption spectra match.

At the triplet-optimized geometries, we calculated the three lowest singlet−singlet (S) and singlet−triplet (T) TDDFT excitations in dichloromethane at the B3LYP/LANL2DZ level, the triplet excited state being related to the emission process. It has to be noticed that the singlet−triplet excitation oscillator strengths are set to zero due to the neglect of spin−orbit coupling in the TDDTF calculations as implemented in G03.

Results and Discussion

Synthesis. Complexes $[Ir(ppy)_2(5\text{-X-1,10-phen})][PF_6]$ (**1**) and $[Ir(pq)_2(5\text{-X-1,10-phen})][PF_6]$ (**2**) were synthesized with phenanthrolines carrying a weak electron-donor substituent (**1a** and **2a**, X = Me), a strong electron-donor substituent (**1b** and **2b**, X = NMe_2), and a strong electron-withdrawing substituent (**1c** and **2c**, X = NO_2). With the aim of investigating the effect of a larger substitution by methyl groups on the phenanthroline, we also synthesized the complexes $[Ir(ppy)_2(4\text{-Me,7-Me-1,10-phen})][PF_6]$ (**3b**), $[Ir(ppy)_2(5\text{-Me,6-Me-1,10-phen})][PF_6]$ (**5**), and $[Ir(ppy)_2(2\text{-Me,9-Me-1,10-phen})][PF_6]$ (**6**). The complex $[Ir(ppy)_2(4\text{-Me-1,10-phen})][PF_6]$ (**7**) was only investigated theoretically by DFT calculations. The complexes $[Ir(ppy)_2(1,10\text{-phen})][PF_6]$ (**1d**) and $[Ir(pq)_2(1,10\text{-phen})][PF_6]$ (**2d**) were taken as references. Finally, to verify the difference between a methyl and a π-delocalized substituent such as a phenyl ring, $[Ir(ppy)_2(4\text{-Ph,7-Ph-1,10-phen})][PF_6]$ (**3a**) was synthesized and studied together with $[Ir(pq)_2(4\text{-Ph,7-Ph-1,10-phen})][PF_6]$ (**4**). All complexes, except **7**, were prepared by a bridge-splitting reaction of the dinuclear precursor $[Ir(ppy)_2(\mu\text{-Cl})]_2$[18] or $[Ir(pq)_2(\mu\text{-Cl})]_2$[18] with the appropriate 1,10-phen ligand added in a stoichiometric amount (see the Experimental Section).

Photophysical Properties. Photophysical data for complexes **1**−**6** are reported in Table 1. All complexes display strong absorption bands between 250 and 290 nm that can be attributed to $\pi-\pi^*$ ligand-centered (LC) transitions typically involving the excitation of electrons from filled π to vacant π^* orbitals of the cyclometalated ppy or pq and phen ligands. Weaker absorption bands at longer wavelengths (in the range of 300−450 nm) have been usually attributed to metal-to-ligand charge transfer (MLCT, arising from the excitation from a filled t_{2g} orbital of the Ir(III) ion to a vacant π^* orbital of the phenanthroline ligand acting as acceptor) and to ligand-to-ligand charge transfer transitions.[9,10,13] A detailed assignment by our DFT investigation of the bands of the absorption spectra of the investigated complexes is given below. The emission spectra of some representative complexes (**1a**, **3a**, and **6**) are shown in Figure 2. The emission maximum can be slightly tuned by varying the nature and number of the phenanthroline's substituents: in CH_2Cl_2 solution it is in the range of 534−592 nm for the investigated complexes (Table 1 and Figure 2). As can be noticed from Figure 2, the emission spectra are broad and

(23) Falciola, L.; Gennaro, A.; Isse, A. A.; Mussini, P. R.; Rossi, M. *J. Electroanal. Chem.* **2006**, *593*, 47.
(24) Ruiz, J.; Astruc, D. *C. R. 'Acad. Sci., Série IIc: Chim.* **1998**, *1* (1), 21.
(25) Noviandri, I.; Brown, K. N.; Fleming, D. S.; Gulyas, P. T.; Lay, P. A.; Masters, A. F.; Phillips, L. *J. Phys. Chem. B* **1999**, *103*, 6713.
(26) Gritzner, G.; Kuta, J. *Pure Appl. Chem.* **1984**, *56*, 461.
(27) Gritzner, G. *Pure Appl. Chem.* **1990**, *62*, 1839.
(28) Ref 22, pp 228−232.
(29) Ref 22, pp 247−252.
(30) Becke, A. D. *Phys. Rev. A* **1988**, *38*, 3098.
(31) Perdew, J. P. *Phys. Rev. B* **1986**, *33*, 8822.
(32) Velde, G. te; Bickelhaupt, F. M.; Baerends, E. J.; Fonseca-Guerra, C.; van Gisbergen, S. J. A.; Snijders, J. G.; Ziegler, T. *J. Comput. Chem.* **2001**, *22*, 931.
(33) Becke, A. D. *J. Chem. Phys.* **1993**, *98*, 5648.
(34) Hay, P. J.; Wadt, W. R. *J. Chem. Phys.* **1985**, *82*, 270.
(35) Miertus, S.; Scrocco, S.; Tomasi, T. *Chem. Phys.* **1981**, *55*, 117.
(36) Frisch, M. J.; Trucks, G. W.; Schlegel, H. B.; Scuseria, G. E.; Robb, M. A.; Cheeseman, J. R.; Montgomery, J. J. A.; Vreven, T.; Kudin, K. N.; Burant, J. C.; Millam, J. M.; Iyengar, S. S.; Tomasi, J.; Barone, V.; Mennucci, B.; Cossi, M.; Scalmani, G.; Rega, N.; Petersson, G. A.; Nakatsuji, H.; Hada, M.; Ehara, M.; Toyota, K.; Fukuda, R.; Hasegawa, J.; Ishida, M.; Nakajima, T.; Honda, Y.; Kitao, O.; Nakai, H.; Klene, M.; Li, X.; Knox, J. E.; Hratchian, H. P.; Cross, J. B.; Bakken, V.; Adamo, C.; Jaramillo, J.; Gomperts, R.; Stratmann, R. E.; Yazyev, O.; Austin, A. J.; Cammi, R.; Pomelli, C.; Ochterski, J. W.; Ayala, P. Y.; Morokuma, K.; Vot, G. A.; Salvador, P.; Dannenberg, J. J.; Zakrzewski, V. G.; Dapprich, S.; Daniels, A. D.; Strain, M. C.; Farkas, O.; Malick, D. K.; Rabuck, A. D.; Raghavachari, K.; Foresman, J. B.; Ortiz, J. V.; Cui, Q.; Baboul, A. G.; Clifford, S.; Cioslowski, J.; Stefanov, B. B.; Liu, G.; Liashenko, A.; Piskorz, P.; Komaromi, I.; Martin, R. L.; Fox, D. J.; Keith, T.; Al-Laham, M. A.; Peng, C. Y.; Nanayakkara, A.; Challacombe, M.; Gill, P. M. W.; Johnson, B.; Chen, W.; Wong, M. W.; Gonzalez, C.; Pople, J. A. *Gaussian 03*, revision B.05; Gaussian, Inc.: Wallingford, CT, 2004.

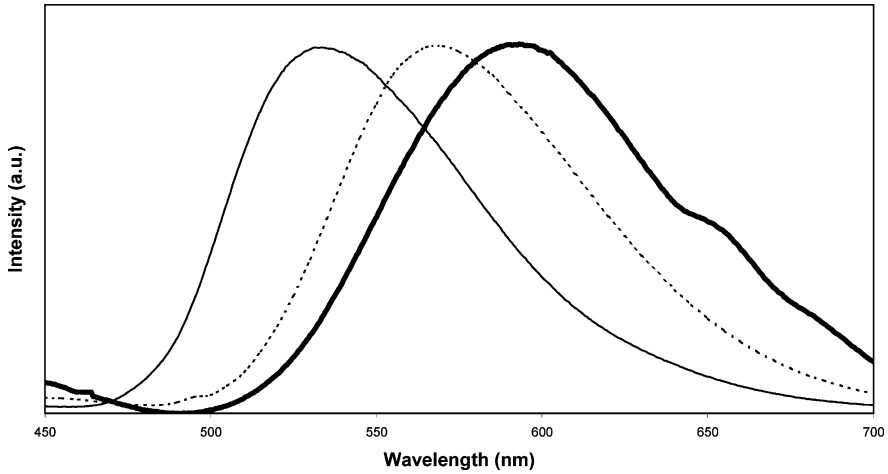

Figure 2. Emission spectra of compounds **1a** (····), **3a** (—), and **6** (−) in CH_2Cl_2 at room temperature.

structureless, evidence of the substantial MLCT character of the emitting state. Indeed, the increasing role of the $\pi-\pi^*$ LC transitions in the emission process is usually associated to a more pronounced vibronic substructure in the emission spectra, even at room temperature.[37] Our TDDFT investigation (see later) has confirmed for some selected complexes the substantial MLCT character of the light-emitting states.

As evidenced in Table 1, the quantum yields of **1**, measured in CH_2Cl_2 solution, strongly depend on the electronic nature of the substituent X. The quantum yield of **1a**, where X is the weak electron-donor methyl group, is quite high ($\Phi = 38\%$ in CH_2Cl_2) whereas that of complex **1b**, where X is a strong electron-donor NMe_2 substituent, is very low ($\Phi = 0.3\%$ in CH_2Cl_2). With a strong electron-withdrawing group such as NO_2 (**1c**) the photoluminescence is below the detection limit. The reference complex (**1d**) has only a rather small quantum yield ($\Phi = 7\%$ in CH_2Cl_2), as previously reported.[10,12] A similar trend is observed for the related **2** complexes (Table 1). Besides, it appears that the presence of two methyl groups on the phenanthroline ligand (e.g., 4-Me,7-Me-1,10-phen, 5-Me,6-Me-1,10-phen, and 2-Me,9-Me-1,10-phen) leads to a continuous decrease of the quantum yield ($\Phi = 26$, 22, and 19% in CH_2Cl_2 solution for complexes **3b**, **5**, and **6,** respectively) when compared with that of the complex bearing **1a**. Complex **3a**, bearing the 4-Ph,7-Ph-1,10-phen ligand, shows a quantum yield ($\Phi = 20\%$ in CH_2Cl_2 solution) slightly lower than the related complex of **3b** with methyl instead of phenyl substituents.

Therefore, we confirmed, with an experimental investigation on a large number of cationic cyclometalated Ir(III) complexes carrying substituted 1,10-phenanthrolines, that the higher quantum yields are shown when the substituents on the phenanthroline ring are alkyl groups, although the increase of the substitution to two methyl substituents does not produce an increase of the quantum yields. The position of the substitution is relevant since complexes **3b**, **5**, and **6** show quite different quantum yields (Table 1).

The emissive lifetimes, measured in deaerated solutions, are in the range of 1.27−4.03 μs (Table 1), in agreement with the values reported for other cationic Ir(III) complexes.[14] From the quantum yields Φ and the lifetimes τ values, the overall radiative and nonradiative rate constants k_r and k_{nr} were calculated for a series of complexes through the equations $k_r = \Phi/\tau$ and $k_{nr} = (1 - \Phi)/\tau$[38] (see Table 1). It appears that the k_r values show a smaller variability compared with that of the k_{nr} values; experimental quantum yields of the various complexes can be analyzed in terms of the different contributions of k_r and k_{nr} for **1a** and **1d** and for **3b** and **2a**, which show the highest quantum yields within the complexes of the series **1**−**3**. According to Einstein's law[39] of spontaneous emission, k_r should be proportional to $\nu^3|\mu|^2$, where μ is the transition dipole moment of the emitting transition and ν^3 is the cube of the emission frequency, while, according to the so-called energy-gap law, k_{nr} should be proportional to $e^{-\nu}$. Therefore k_{nr} is expected to decrease significantly by increasing the emission frequency.[40] For the investigated complexes (see Table 1), all emitting in a rather similar range of the emission frequency, comparable k_r values are found; this in turn relates to similar $|\mu|^2$ values, confirming a common nature of the emitting excited states.

Complexes **1a** and **2a** show comparably higher quantum yields than all the other complexes, mainly as a result of the relatively low k_{nr} values compared with, e.g., **1d** and **3b** (Table 1). However, while for **3b** the rather high k_{nr} value is partially compensated by the highest k_r value among all the investigated complexes, providing a quantum yield of 26%, for **1d**, the low k_r value leads to a quantum yield of 7%. The energy gap law is effectively obeyed by **1d**, **1a**, and **2a** (Table 1 and Supporting Information) while the higher k_{nr} value of **3b** is not easily correlated with the k_{nr} values of

(37) (a) Colombo, M. G.; Hauser, A.; Güdel, H. U. *Inorg. Chem.* **1993**, *32*, 3088. (b) Colombo, M. G.; Brunold, C. T.; Riedener, T.; Güdel, H. U.; Förtsch, M.; Bürgi, H.-B. *Inorg. Chem.* **1994**, *33*, 545.

(38) Straughan, B. P.; Walker, S. *Spectroscopy*; Science Paperbacks; Chapman & Hall, London, 1976; Vol. 3.

(39) (a) Strickler, S. J.; Berg, R. A. *J. Chem. Phys.* **1962**, *37*, 814. (b) Einstein, A. *Phys. Z.* **1917**, *18*, 121.

(40) (a) Kober, E. M.; Caspar, J. V.; Lumpkin, R. S.; Meyer, T. J. *J. Phys. Chem.* **1986**, *90*, 3722. (b) Henry, B. R.; Siebrand, W. In *Organic Molecular Photophysics;* Birks, J. B., Ed.; Wiley, New York, 1973; Vol. 1, Chapter 4. (c) Freed, K. F.; Jortner, J. *J. Chem. Phys.* **1970**, *52*, 6272. (d) Bixon, M.; Jortner, J. *J. Chem. Phys.* **1968**, *48*, 715.

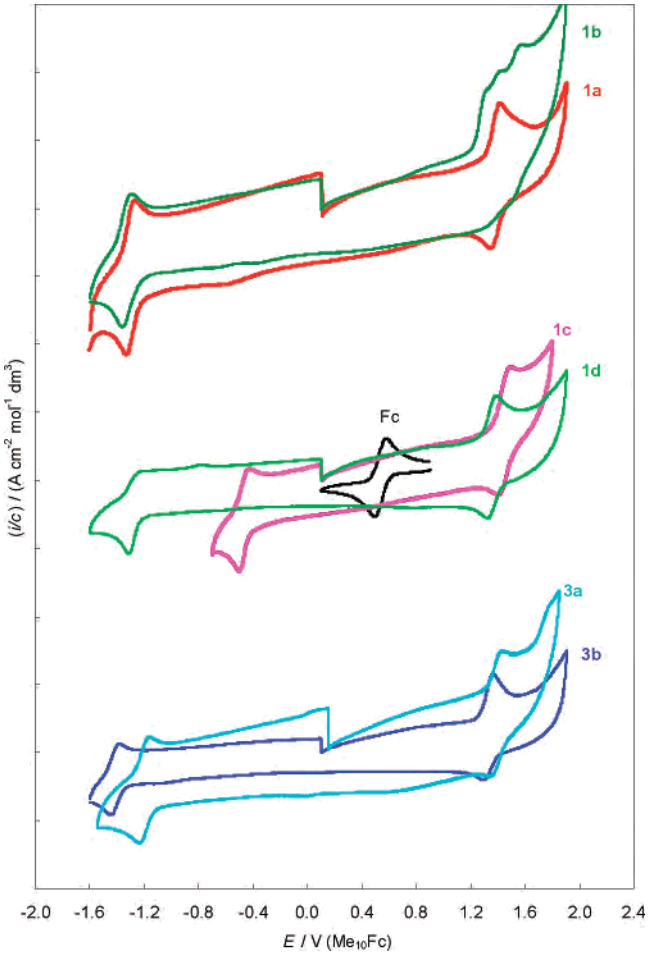

Figure 3. CV patterns of compounds **1a**−**d** and **3a** and **3b**, working at (1.8−2.8) × 10^{-4} M concentrations in CH_3CN + 0.1 M $[NBu_4]PF_6$ and with a GC electrode. The CV pattern of the reference model compound ferrocene (Fc), as a standard for a monoelectronic chemically and electrochemically reversible reaction, is also reported.

1d, **1a**, and **2a**. Overall, the relative quantum yields of the investigated complexes are mainly controlled by nonradiative deactivation processes, since, in contrast with the rather limited variations of k_r (in the range of (0.5−1.8) × 10^5 s^{-1}), significant variations of k_{nr} values (in the range of (1.64−7.1) × 10^5 s^{-1}) are found. The wider variation range of k_{nr} values probably originates in the significant effect of the nature and position of substituents on the phenanthroline ring deformation motions, which might control the nonradiative pathway of decay.

Electrochemical Properties. Figure 3 shows the CV pattern of the investigated Ir(III) complexes working in a 1.8−2.8 10^{-4} M range of concentration in CH_3CN solutions added with 0.1 M $[NBu_4]PF_6$ and working with a GC electrode (see Experimental Section for details). The CV pattern of the reference model compound ferrocene, used as the standard for a monoelectronic chemically and electrochemically reversible reaction, is also reported in Figure 3. In Table 2, the oxidation and reduction potentials are given, together with the reversibility parameters (the half-peak width ($E_p - E_{p/2}$) and the distance between the forward and backward peak potential ($E_{p,f} - E_{p,b}$)[22]). Half-wave potentials from the "stationary" steplike waves obtained by means of convolution analysis of the original CV characteristics are also reported. Moreover, in Table 2 the HOMO−LUMO energy gaps, calculated from the difference between the anodic and cathodic peak potentials, are also reported and compared with those calculated by a DFT theoretical approach (see below).

All compounds show a chemically and electrochemically reversible anodic peak, with the exception of compounds **1b** and **2b**, carrying a NMe_2 group, which show a complex oxidation signal composed by three subsequent multielectronic and very close peaks at 1.33, 1.42, and 1.58 V (vs $Me_{10}Fc$, where Fc is ferrocene), suggesting that the NMe_2 group is probably also involved in the oxidation process. At low scan rates (<0.1 V s^{-1}), a loss of chemical reversibility occurs, suggesting a chemical reaction following the oxidation processes. Moreover, all the compounds show in the reduction part a chemically and electrochemically reversible cathodic peak generally followed by other peaks (see Figure 3 and the Supporting Information), different in intensity, shape, and number, depending on the compound.

As reported for these types of Ir(III) complexes,[2c,4,9,41] the oxidation processes are linked to metal-centered orbitals with a contribution from the phenyl part of cyclometalated fragments (ppy or pq), which usually lead to an increased loss of electrochemical reversibility. On the other hand, reduction processes are assigned to orbitals centered mainly on the Ir−phen fragment.[2c,4,9,24] Both these assignments are confirmed by our DFT calculations (see below). The presence of one or two weak electron-donor groups (CH_3) on the phenanthroline ring shifts, as expected, the reduction peak potentials to lower values with the stronger effect (130 mV) for compound **3b**, bearing two methyl groups in positions 4 and 7. The effect of the methyl groups is remarkably lower on the oxidation peak, where a slight anticipation of the peak potential (20 mV) can be perceived only in the presence of two methyl groups. However, in compound **6**, we have a significant perturbing effect (see Table 2), probably caused by the steric influence of the two methyl groups in positions 2 and 9 on the availability of orbitals of the Ir site, as confirmed by DFT calculations (see below).

The presence of a strong electron-donor (NMe_2) or electron-acceptor (NO_2) group on the phenanthroline ligand significantly shifts the oxidation peak potentials to lower or higher values (60−120 mV), respectively, according to the electron enrichment/depletion of the metal-centered redox site (in Table 2, compare **1b**, **2b** and **1c**, **2c** with compound **1d**) due to the quite different donor properties of the phenanthroline ligand. Symmetrically, while the presence of NMe_2 shifts the reduction peak potential to more negative values, due to the higher electron density on the phenanthroline ligand, the opposite effect is observed by the presence of the NO_2 electron-withdrawing group, resulting in a dramatic anticipation of the reduction peak potentials

(41) Calogero, G.; Giuffrida, G.; Serroni, S.; Ricevuto, V.; Campagna, S. *Inorg. Chem.* **1995**, *34*, 541.

Table 2. Oxidation E_A and Reduction E_C Potentials (against $Me_{10}Fc$), Reversibility Parameters, Half-Wave Potentials (as Volts) of the Investigated Ir(III) Complexes on a GC Electrode, in a 1.8−2.8 10^{-4} M Range of Concentrations in CH_3CN Solution Added with 0.1 M $[NBu_4]PF_6$ as Supporting Electrolyte. HOMO−LUMO Energy Gaps (Band Gap), Obtained from the Difference between the Anodic and Cathodic Peak Potentials, Compared with Those Calculated by DFT Calculations (ΔE H−L), Are Also Reported

		oxidation				reduction					
compound	MW	E_A/V	$E_p - E_{p/2}$/V	$E_{p,f} - E_{p,b}$/V	$E_{1/2}$/V	E_c/V	$E_p - E_{p/2}$/V	$E_{p,f} - E_{p,b}$/V	$E_{1/2}$/V	band gap	ΔE H−L
1a	839.74	1.42	0.053	0.059	1.39	−1.32	0.059	−0.063	−1.28	2.74	3.16
1b	868.82	1.33	0.058			−1.36	0.074	−0.068	−1.31	2.69	3.24
1c	870.75	1.48	0.061	0.070	1.44	−0.49	0.041	−0.071	−0.48	1.97	2.08
1d	825.4	1.39	0.061	0.063	1.36	−1.30	0.046	−0.067	−1.28	2.69	3.18
2a	939.86	1.42	0.054	0.060	1.40	−1.32	0.058	−0.064	−1.28	2.74	3.16
2b	968.94	1.33				−1.37	0.062	−0.069	−1.34	2.70	3.24
2c	970.87	1.51	0.061	0.068	1.46	−0.51	0.041	−0.047	−0.49	2.02	2.07
3a	977.93	1.43	0.056	0.068	1.39	−1.22	0.065	−0.050	−1.20	2.65	3.15
3b	853.2	1.37	0.055	0.069	1.35	−1.43	0.053	−0.058	−1.40	2.80	3.27
4	1080.12	1.45	0.060	0.052	1.42	−1.22	0.059	−0.060	−1.20	2.67	3.14
5	853.2	1.39	0.060	0.062	1.35	−1.36	0.060	−0.059	−1.32	2.75	3.18
6	853.2	1.48	0.060	0.094	1.43	−1.41	0.055	−0.086	−1.37	2.89	3.34

Table 3. Selected Optimized Bond Lengths (Å) and Angles (deg) for Complexes **1**−**7** (Optimized Parameters for the Triplet-State Geometries Are Reported in Parentheses for Selected Complexes)

	$Ir-N_{ppy}$	$Ir-Cp_{py}$	$C_{ppy}-C_{ppy}$	$Ir-N_{phen}$	$C_{phen}-C_{phen}$	$C_{ppy}-Ir-N_{ppy}$	$N_{phen}-Ir-N_{phen}$
1a	2.059	2.009	1.451	2.165	1.428	80.2	76.7
	(2.057)	(1.980)	(1.447)	(2.177)	(1.406)	(81.1)	(76.3)
1b	2.058	2.010	1.451	2.157	1.425	80.2	76.4
1c	2.060	2.009	1.451	2.158	1.431	80.2	76.4
1d	2.060	2.009	1.451	2.164	1.428	80.3	76.7
	(2.056)	(1.989)	(1.449)	(2.170)	(1.407)	(81.0)	(76.5)
3a	2.058	2.009	1.451	2.155	1.429	80.2	76.5
	(2.058)	(1.980)	(1.446)	(2.170)	(1.408)	(81.05)	(76.1)
3b	2.058	2.009	1.451	2.162	1.431	80.2	76.3
	(2.119)	(1.973)	(1.441)	(2.208)	(1.416)	(80.7)	(74.5)
5	2.059	2.009	1.451	2.150	1.425	80.3	76.7
6	2.058	2.011	1.449	2.247	1.436	80.2	76.0
7	2.060	2.010	1.451	2.163	1.429	80.2	76.6
	$Ir-N_{ppy}$	$Ir-C_{ppy}$	$C_{ppy}-C_{ppy}$	$Ir-N_{bpy}$	$C_{bpy}-C_{bpy}$	$C_{ppy}-Ir-N_{ppy}$	$N_{bpy}-Ir-N_{bpy}$
X-ray[a]	2.057(6)	2.015(7)	−	2.151(6)	−	80.1(3)	76.3(3)
X-ray[b]	2.057(6)	1.997(6)	−	2.262(5)	−	84.6(2)	75.44(18)
	2.056(5)	2.014(6)		2.217(5)			
	$Ir-N_{pq}$	$Ir-C_{pq}$	$C_{pq}-C_{pq}$	$Ir-N_{phen}$	$C_{phen}-C_{phen}$	$C_{pq}-Ir-N_{pq}$	$N_{phen}-Ir-N_{phen}$
2a	2.1275	1.9995	1.446	2.180	1.426	79.65	75.9
	(2.117)	(2.119)	(1.442)	(2.208)	(1.412)	(80.7)	(74.6)
2b	2.117	2.000	1.446	2.177	1.424	79.75	75.5
2c	2.119	2.001	1.446	2.181	1.429	79.7	75.4
4	2.128	2.000	1.445	2.178	1.428	79.8	75.9
	(2.119)	(1.973)	(1.441)	(2.208)	(1.416)	(80.7)	(74.5)

[a]X-ray data refer to those reported for $[Ir(ppy)_2(4,4'-C_9H_{19}-2,2'-bipyridine)]^+$ in ref 9a. [b]X-ray data refer to those reported for $[Ir(ppy)_2(6,6'-diphenyl-^tBu-bipyridine)]^+$ in ref 9b.

(810 mV). In this latter case, however, the reduction process might be centered on the NO_2 group.[42]

Furthermore, the substitution of ppy with pq (compare **1a**−**c** and **3a** with **2a**−**c** and **4**, respectively) more significantly shifts, as expected, the oxidation potentials to positive values (shift of 20−30 mV), while the reduction potentials are shifted to slightly more negative values (shift of only 10 mV), i.e., in both cases toward the higher energy required for the oxidation or the reduction, respectively. These effects could be ascribed to a screening effect of the bulkier pq ligand (with respect to the ppy one) on the electron transfer, which must be more relevant on the oxidation process that involves both the cyclometalated ligands and the Ir center.

Finally, a good linear correlation ($r^2 = 0.98$) between the experimental and the DFT-calculated HOMO−LUMO energy gap was obtained (see Table 2 and the Supporting Information).

DFT and TDDFT Calculations. To provide more detailed insight into the electronic energy levels and nature of the electronic transitions controlling the electrochemical and optical properties, we performed DFT calculations on all the cationic iridium complexes investigated experimentally and also on complex **7.** We optimized the singlet ground-state geometries of all the various cationic complexes and the lowest triplet excited-state geometries of **1a**, **1d**, **2a**, **3a**, **3b**, and **4** complexes. Selected optimized geometrical parameters of the ground and some triplet states are collected in Table 3 and compared to the available structural data obtained from an X-ray investigation of the related complex $[Ir(ppy)_2(4,4'-C_9H_{19}-2,2'-bipyridine)]^+$ [9a] and $Ir(ppy)_2(6,6'-diphenyl-^tBu-bipyridine)]^+$.[9b] Even though these complexes carry the bipyridine ligand instead of the phenanthroline ligand, our optimized geometrical parameters are in excellent agreement

(42) (a) Annoni, E.; Pizzotti, M.; Ugo, R.; Quici, S.; Morotti, T.; Bruschi, M.; Mussini, P. *Eur. J. Inorg. Chem.* **2005**, 3857. (b) Morotti, T.; Pizzotti, M.; Ugo, R.; Quici, S.; Bruschi, M.; Mussini, P.; Righetto, S. *Eur. J. Inorg. Chem.* **2006**, 1743.

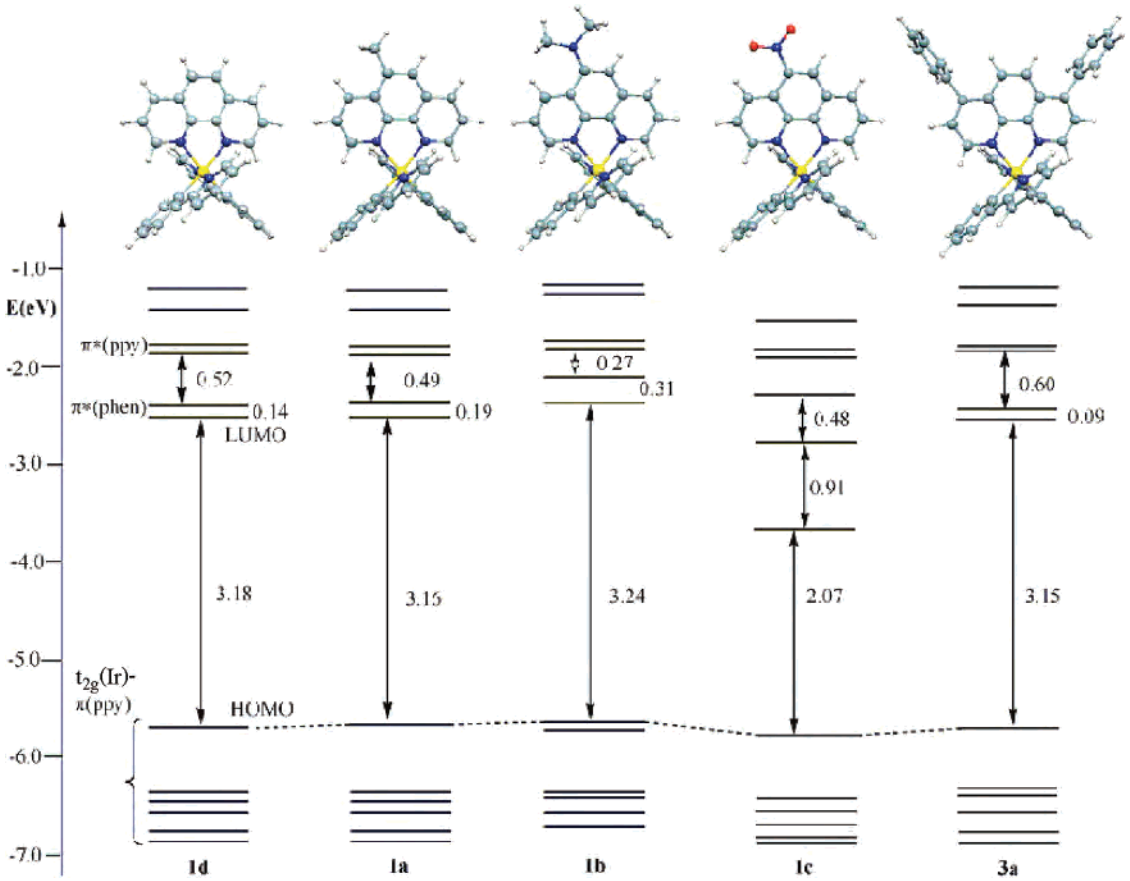

Figure 4. Schematic representation of the frontier molecular orbitals of complexes **1a**−**d** and **3a** in acetonitrile solution

with the X-ray data. For instance, for the ppy complexes, we calculated Ir−N(ppy), Ir−C(ppy), and Ir−N(phen) bond distances of 2.057−2.060, 2.008−2.011, and 2.150−2.166 Å compared to X-ray experimental values[9] of 2.057(6), 2.015(7), and 2.151(6) Å, respectively. Interestingly, for complex **6**, we evidenced a significantly lengthened Ir−N(phen) bond distance (2.25 vs 2.16 Å for **6** and **1d/3b**, respectively). This effect is due to the presence of two methyl substituents in the 2 and 9 positions, which sterically perturbs the metal coordination sphere, as also shown by our electrochemical investigation, thus producing a strain on the Ir−N(phen) bond. A similar effect was found for the X-ray structure of $Ir(ppy)_2$(6,6′-diphenyl-^{t}Bu-bipyridine)]$^+$,[9b] due to the presence in this case of bulky phenyl substituents in the 2 and 9 positions. Bond angles show minimal variations among the complexes investigated and are in good agreement with X-ray experimental values.[9] Compared with the ppy complexes, the corresponding pq complexes show longer Ir−N(pq and phen) and shorter Ir−C(pq) bond distances. This effect is magnified for the Ir−N bonds, which are on average ca. 0.05 Å longer than those of the corresponding ppy complex as a result of the hindrance exerted by the more bulky pq ligand, as clearly shown in the case of the sterically crowded complex **4** (see Table 3). Interestingly, for some complexes, we have evidenced a correlation between the steric hindrance around the metal center due to the ppy ligand and the ratio of the deaerated/not deaerated excited-state lifetimes (see notes of Table 1). Indeed, the more sterically crowded complex **4** shows a decreased deaerated/not deaerated lifetimes ratio (3.57) compared with **3a** (3.97), which in turn has a lower ratio than, e.g., **1d** (6.89), which is the less sterically hindered complex among those investigated. This behavior might be due to the shielding of the metal coordination sphere by more bulky ligands, which in turn protect the metal center of the octahedral complex in the excited state from interacting with triplet molecular oxygen.

On the optimized geometries, we performed single-point calculations in dichloromethane and acetonitrile solutions. The results, in terms of frontier orbitals, are reported in Figures 4−6 and in the Supporting Information. The two solvents were chosen because they are those experimentally employed for the photophysical and electrochemical measurements, respectively. In Figure 4, for the complexes bearing the ppy ligands, the effect of a substituent in position 5 of the phenanthroline (**1a**−**c**) and of two phenyl substituents in positions 4 and 7 (**3a**) is reported together with the frontier orbitals of the reference complex **1d.**

For complexes **1a**−**d** and **3a**, the HOMO is, as found for the related Ir(III) complexes, an antibonding combination of Ir(t_{2g}) and ppy(π) orbitals.[4,10,13,15,16] The HOMO is followed, in order of decreasing energy, by two additional combinations of Ir(t_{2g}) and ppy(π) orbitals, with decreasing ppy character. However, for complex **1b**, the HOMO-1 is a π-bonding orbital of the NMe_2-substituted phenanthroline, which lies close to the HOMO, as a result of the increased electron donation of the NMe_2 group on the phenanthroline ring. This low-energy orbital, also obtained for the related pq complex **2b**, might be responsible for the complex

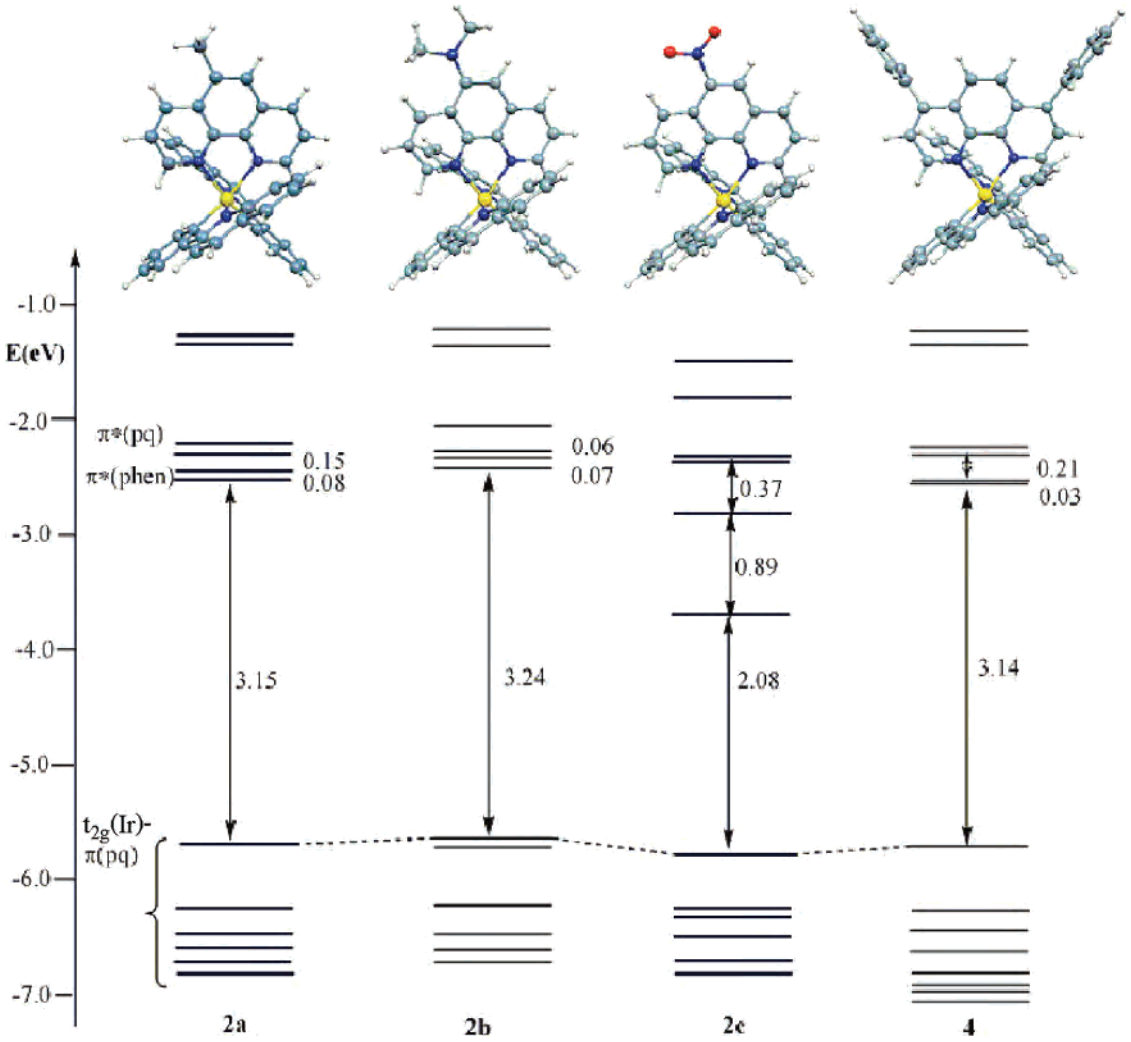

Figure 5. Schematic representation of the frontier molecular orbitals of complexes **2a**−**c** and **4** in acetonitrile solution

oxidation peaks observed experimentally (Table 2). The LUMO of all the complexes **1a**−**d** and **3a** is a π^* orbital localized on the phenanthroline ligand acting as an acceptor.[4,10,13,15,16] For these complexes, with the exception of **1c** (see below), the LUMO is followed by a second phenanthroline π^* orbital (LUMO+1), whose energy relative to the LUMO depends upon the substituent, and at higher energies by a couple of ppy π^* orbitals (LUMO+2 and LUMO+3) almost degenerate, irrespective of the substituent on the phenanthroline ligand. This electronic structure is not affected by a change of solvent, even though a general energy downshift of both occupied and unoccupied orbitals is calculated for dichloromethane compared with that of acetonitrile (see the Supporting Information).

The presence of a methyl group in position 5 does not substantially affect the electronic structure with respect to the reference complex **1d**, while the presence in position 5 of a stronger donor such as the NMe_2 group (**1b**) leads to a destabilization of the HOMO and to major effects on the LUMO/LUMO+1 and LUMO+1/LUMO+2 separations. The pattern of the unoccupied orbitals of complex **3a** with phenyl groups in positions 4 and 7 of the phenanthroline ligand is similar to that of the reference **1d** complex, but with the smallest LUMO/LUMO+1 and largest LUMO+1/LUMO+2 gaps, as a result of the phenanthroline π^* LUMOs stabilization due to some π conjugation with the phenyl ligands. For **1c**, the strongly electron-withdrawing NO_2 group leads to a dramatic stabilization of all the phenanthroline π^* orbitals, which ultimately leads to a drastic reduction by more than 1 eV of the HOMO−LUMO gap. The LUMO, LUMO+1, and LUMO+2 orbitals become phenanthroline π^* orbitals strongly mixed with the NO_2 orbitals.

In Figure 5, the electronic structure of the phenanthroline complexes bearing two pq ligands (**2a**−**c** and **4)** is reported, to be compared to the electronic structure of the corresponding complexes with two ppy ligands (**1a**−**c** and **3a)**. The pattern of the occupied orbitals is essentially the same in the two series of complexes, with the HOMO being a combination of Ir(t_{2g}) and pq(π) orbitals. Complex **2b**, due to the presence of a NMe_2 group, shows a HOMO-1 of π-bonding phenanthroline character inserted just below the HOMO. Also, the pattern of unoccupied orbitals is similar to that of the corresponding ppy complexes, even though sizable differences in their relative energies are calculated. In particular, the LUMO and LUMO+1 phenanthroline π^* orbitals are now almost degenerate, reflecting a more-symmetrical coordination sphere. In addition, the pq-based π^* LUMO+2/LUMO+3 orbitals are considerably stabilized

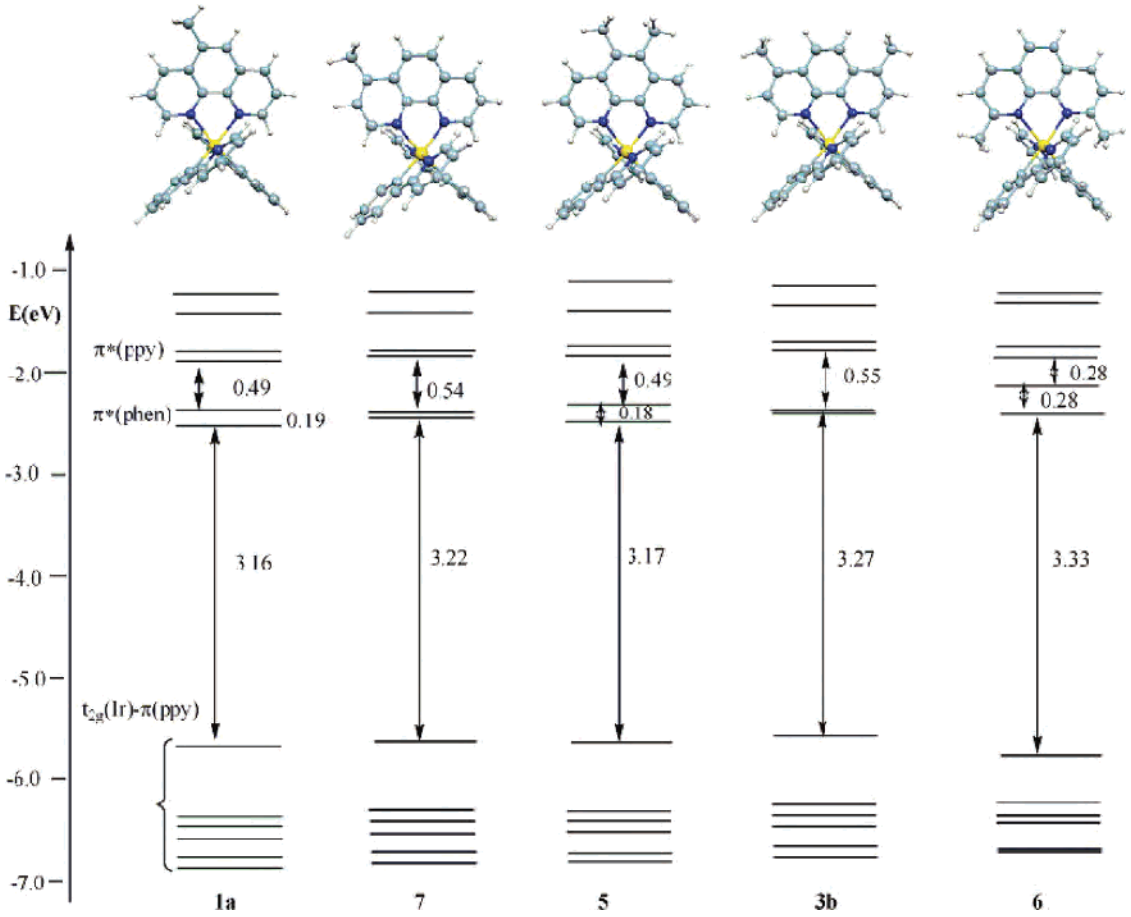

Figure 6. Schematic representation of the frontier molecular orbitals of complexes **3b** and **5**−**7** compared to those of complex **1a** in acetonitrile solution.

with respect to the corresponding ppy-π* LUMO+2/LUMO+3 orbitals, lying about 0.4−0.5 eV below, as an effect of the more-extended π delocalization of the pq ligand. Such an effect is particularly pronounced in the case of the NO_2-substituted complex **2c**, for which extensive mixing of π* phenanthroline and π* pq orbitals is calculated.

The effect of the number of methyl substituents and of their position on the phenanthroline ligand is reported in Figure 6. Moving the methyl substituent from the 5 (**1a**) to the 4 (**7**) position does not significantly affect the electronic structure. Also, for complex **5**, with two methyl groups in positions 5 and 6, we notice that, compared to **1a**, no substantial change of the electronic structure occurs, apart from a slightly destabilization of the LUMO. For complex **3b**, dimethylated in positions 4 and 7, a slight LUMO destabilization is calculated, which brings the LUMO and LUMO+1 orbitals to become almost perfectly degenerate, and leads to a HOMO−LUMO gap increase of ca. 0.1 eV. Complex **6** shows a sizable stabilization of the HOMO, reflecting the effect on the t_{2g} metal orbitals accomplished by the presence of two methyl substituents in positions 2 and 9, which reduces the donation from the phenanthroline ligand, leading to substantial elongated Ir−N bond. The final result is an overall increase of the HOMO−LUMO gap and an increase of the LUMO/LUMO+1 splitting.

Comparison of the calculated HOMO−LUMO gap with the electrochemical energy difference between redox potentials shows good correlation (Table 2 and Supporting Information), even though a quantitative agreement between the HOMO−LUMO gap and the energy difference between redox potentials is not to be expected. In fact, we are not taking into account the relaxation of the electronic structure upon the population/depopulation of the unoccupied/occupied orbitals (see the Supporting Information).

For complexes **1a**, **1d**, **3a**, and **3b**, with the higher quantum yields (Table 1), we simulated the absorption spectra by computing the lowest 70 excitation energies by TDDFT in dichloromethane solution, thus allowing us the simulation of a large portion of the spectrum, below 250 nm. Given the similarity of the absorption spectra for these complexes, we discuss in detail only the absorption spectrum of **1a** (see the Supporting Information for complexes **1d**, **3a**, and **3b**). It has to be stressed here that, even though singlet−triplet excitations can be calculated, their oscillator strengths are set to zero due to the neglect of spin−orbit coupling in the TDDTF calculations, so that these transitions do not contribute to the overall spectral profile. This should represent an acceptable approximation in the high-energy region dominated by the more intense singlet−singlet transitions, while the contribution of singlet−triplet excitation might become relevant in the low-energy portion of the spectrum.

A comparison of the calculated and experimental spectra for complex **1a** in dichloromethane solution is reported in Figure 7. As can be observed, the agreement between theory and experiment is good, both in terms of absolute band positions and relative intensities, especially considering the

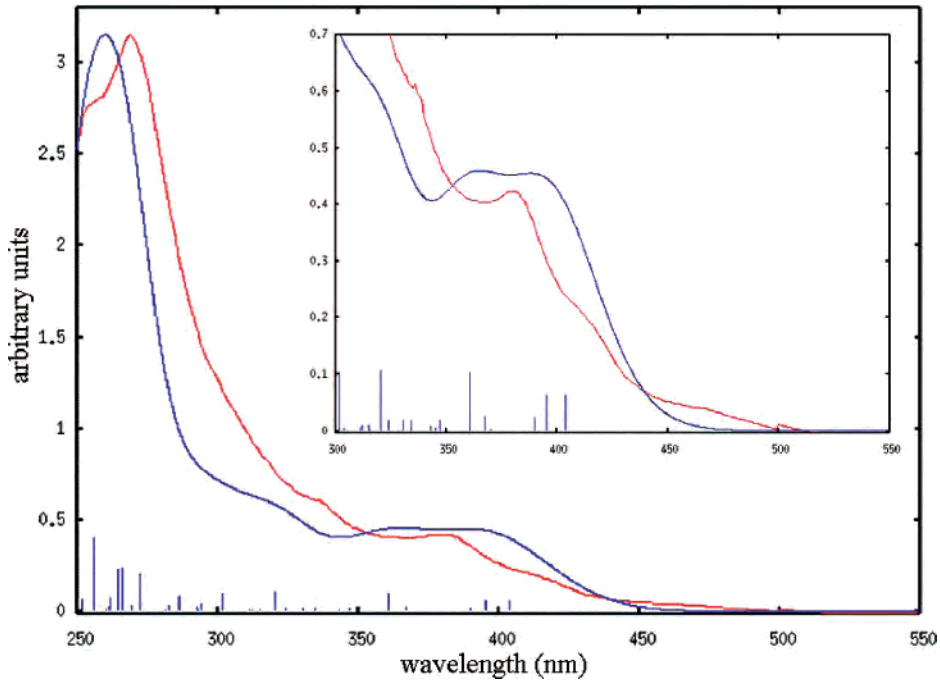

Figure 7. Comparison between the experimental (red line) and computed (blue line) absorption spectra of the **1a** complex in dichloromethane solution. Inset: detail of the spectra in the 300−550 nm range. The experimental spectrum has been rescaled so that the intensity of the 268 nm band of the experimental spectrum matches the theoretical main feature.

rather limited dimensions of the basis set and the neglect of spin−orbit coupling in the excitation energies. The experimental absorption spectrum shows an intense feature at 268 nm with a shoulder at 333 nm. At longer wavelengths, a less-intense absorption band is found at 377 nm, with a shoulder at 410 nm and a tail extending above 450 nm. The calculated absorption spectrum nicely reproduces the main features of the experimental one, with an overall deviation within 0.15 eV between the main calculated and experimental values. In particular, we calculate an intense band at 260 nm with a shoulder at 322 nm, in excellent agreement with the 268 and 333 nm experimental values. At longer wavelengths, we calculate two overlapping absorptions at 366 and 399 nm, which can be related to the 377 nm band of the experimental absorption spectrum and to its 410 nm shoulder, respectively.

Inspection of the TDDFT eigenvectors allows the assignment of the main spectral features in terms of their singly occupied to virtual molecular orbital contributions. The lowest excitation energies of low intensity for **1a** are calculated to be of singlet−triplet character and are located at 524 and 466 nm, with the corresponding lowest singlet−singlet excitations, of negligible intensity, found at 519 and 465 nm. The 524 and 519 nm excitations correspond to HOMO−LUMO transitions, followed at higher energy by the 466 and 465 nm excitations of HOMO-1−LUMO character. These two couples of low-intensity transitions therefore have MLCT character, with arriving states localized on the phenanthroline ligand. The lowest-energy transitions of sizable intensity are calculated at 404 and 395 nm (f = 0.064 and 0.064, respectively); the 404 nm excitation is of HOMO−LUMO+2 character and is therefore still a MLCT transition, with arriving states localized on the phenylpyridine ligands, while the 395 nm feature has mainly HOMO-1−LUMO character, therefore being a MLCT transition with arriving states on the phenanthroline ligand. These latter two transitions give rise to the feature of the simulated spectrum at 399 nm, which can be related to the 410 nm shoulder found experimentally. The band experimentally found at 377 nm appears to be related to an intense transition calculated at 361 nm (f = 0.101) composed by almost equal contributions of HOMO-2−LUMO+1 and HOMO-3−LUMO excitations, therefore showing substantial mixing of MLCT and $\pi-\pi^*$ character, with arriving states localized on the phenanthroline ligand. Moving to higher energies, the MLCT contribution decreases, so the band measured at 268 nm corresponds to a series of intense, almost overlapping $\pi-\pi^*$ excitations of both the phenanthroline and phenylpyridine ligands, giving rise to an overall feature at 260 nm.

To gain insight into the nature of the emitting excited states of the investigated complexes, we performed TDDFT calculations in a dichloromethane solution on the optimized lowest triplet excited-state geometry of some selected compounds; in particular, we investigated complexes **1a**, **1d**, **2a**, **3a**, **3b**, and **4**. The triplet-optimized geometries are not too different for all the above complexes from those of the ground singlet state (see Table 3). Taking **1a** as an example, the largest difference is observed for the C−C(phen) bond distances connecting the two pyridine units of the phen moiety, which decreases from 1.428 to 1.406 Å. This is due to the bonding interaction between the p orbitals of the two connecting carbon atoms characterizing the LUMO orbital. Slight differences are computed also for the Ir−N(phen) and Ir−C(ppy) bond distances which, respectively, increase and decrease compared to their value in the ground-state geometry. The reinforced Ir−C interaction in the excited state is due to the depopulation of the HOMO orbital based on Ir and ppy contributions, which in turn weakens the Ir−N(phen)

Table 4. Lowest Singlet−Singlet (S) and Singlet−Triplet (T) Excitation Energies (nm; eV) and Composition in Terms of Molecular Orbital Excitations for **1a**, **1d**, **2a**, **3a**, **3b**, and **4** Calculated at the Triplet-State-Optimized Geometries[a]

	Em. exp (nm; eV)	T_1	T_2	T_3	S_1	S_2	S_3
1a	559; 2.218	600; 2.067 HOMO−LUMO	488; 2.543 HOMO−LUMO+1	478; 2.593 HOMO−LUMO+2	592; 2.093 (0.0003) HOMO−LUMO	486; 2.551 (0.0001) HOMO−LUMO+1	429; 2.893 (0.0785) HOMO−LUMO+2
1d	575; 2.156	594; 2.086 HOMO−LUMO	488; 2.539 HOMO−LUMO+1	478; 2.592 HOMO−LUMO+2	585; 2.121 (0.0003) HOMO−LUMO	485; 2.554 (0.0000) HOMO−LUMO+1	422; 2.937 (0.0765) HOMO−LUMO+2
2a	556; 2.230	582; 2.130 HOMO−LUMO	555; 2.235 HOMO−LUMO+2	544; 2.279 HOMO−LUMO+1/ HOMO−LUMO+3	572; 2.167 (0.0008) HOMO−LUMO	512; 2.421 (0.0010) HOMO−LUMO+1	505; 2.455 (0.0762) HOMO−LUMO+2
3a	592; 2.094	600; 2.068 HOMO−LUMO	501; 2.472 HOMO−LUMO+1	479; 2.587 HOMO−LUMO+2	590; 2.102 (0.0004) HOMO−LUMO	498; 2.489 (0.0001) HOMO−LUMO+1	427; 2.904 (0.0748) HOMO−LUMO+2
3b	552; 2.246	565; 2.195 HOMO−LUMO	501; 2.475 HOMO−LUMO+1	483; 2.565 HOMO−LUMO+2	557; 2.228 (0.0004) HOMO−LUMO	498; 2.488 (0.0000) HOMO−LUMO+1	432; 2.868 (0.0782) HOMO−LUMO+2
4	562; 2.206	580; 2.138 HOMO−LUMO	560; 2.215 HOMO−LUMO+2	558; 2.224 HOMO−LUMO+1/ HOMO−LUMO+3	567; 2.186 (0.0015) HOMO−LUMO	522; 2.373 (0.0004) HOMO−LUMO+1	508; 2.440 (0.0711) HOMO−LUMO+2

[a] The oscillator strengths of the singlet−singlet transitions are reported in parentheses. Experimental values (Em. exp) of the emission maxima are reported for comparison.

bonds trans to the Ir−C bonds. The singlet ground-state electronic structure calculated at the triplet geometry shows the same orbital pattern calculated for the ground-state geometry, even though changes in the orbital energies take place.

The energy and character of the three computed lowest excited singlet states S_1, S_2, and S_3 and triplet states T_1, T_2, and T_3 for **1a**, **1d**, **2a**, **3a**, **3b**, and **4** are reported in Table 4. At the triplet-optimized geometries, the lowest excited state is of ^{3}MLCT character (S_0-T_1 in Table 4), involving a single orbital excitation from the Ir(t_{2g})/ppy(π)- or Ir(t_{2g})/pq(π)-based HOMO orbital to the phen π^*-based LUMO orbital. The lowest singlet excited state (S_0-S_1) has the same MLCT character and lies close to the ^{3}MLCT state, showing in all cases negligible oscillator strength. The comparison of calculated lowest excitation energies with experimental emission maxima is not straightforward, since the latter are broad and structureless and it is therefore quite difficult to localize the E_{0-0} transition, which can be estimated by the lowest excitation energy calculated by TDDFT. Nevertheless, the calculated T_1 excitation energies are in good agreement with experimental emission maxima: the largest discrepancy is calculated for **1a**, for which a slight red-shifted value (0.151 eV) is calculated (see Table 4) and small discrepancies (between 0.02 and 0.06 eV) in the energy trends between calculated and measured values are found. These deviations, which are well below the accuracy of the theoretical setup, might also be related to an inhomogeneous comparison between theory and experiment, as discussed above. We notice, in general, that a substantial stabilization of the excited states takes place at the triplet-optimized geometry, compared with the singlet ground state ones. For the lowest singlet and triplet excited states, this stabilization energy amounts to ca. 0.3 eV while more limited variations, within ca. 0.1 eV, are calculated for the second lowest excitation energies.

Finally, it is interesting to compare our results, obtained in the context of the present investigation, with the experimental[8] and theoretical results[15a,d] reported for the prototype [Ir(2-phenylpyridine)$_2$(4,4′-*tert*-butyl-2,2′-bipyridine)]$^+$ complex, hereafter **8**: in particular, it seems worthwhile to compare complex **8**, bearing a doubly substituted bipyridine ligand with alkyl groups, with **3b**, which shows a phenanthroline with two alkyl substituents in the same positions. Complex **8** in acetonitrile shows a slightly red-shifted emission wavelength compared with **3b** in dichloromethane, 581 vs 552 nm, respectively, in line with DFT/TDDFT calculations performed in acetonitrile on **8**,[15a,d] showing a lowest S_0-T_1 transition at 583 nm, as compared with the 565 nm value calculated here for **3b** in dichloromethane. The slightly red-shifted emission observed for **8** is entirely due to the slight LUMO stabilization (by 0.11 eV) compared to **3b**, the HOMO lying at the same energy in both species in acetonitrile solution. Relevant differences between **3b** and **8** are found, on the other hand, when looking at the emission lifetimes, even though the two complexes show similar quantum yields (0.23[8] vs 0.26 for **8** and **3b**, respectively) and the two data sets have been obtained in different solvents; for **3b**, we measure an emission lifetime of 1.43 μs, while a value of 0.557 μs was reported for **8**.[8] Given the similar quantum yields, this difference translates into a comparable difference in the radiative and nonradiative rate constants (1.82 and 5.17 vs 4.31 and 13.6 10^5 s^{-1} for **3b** and **8**, respectively). Since in both complexes the lowest excited state is of ^{3}MLCT character, originating from the same Ir−ppy HOMO, the observed differences might reside in the different solvents used in the experiments and/or in the different Franck−Condon factors exhibited by metallorganic complexes bearing phenanthroline and bipyridine ligands.[40a]

Conclusions

This work shows how the nature and number of substituents on the phenanthroline can significantly influence some of the photochemical properties of [Ir(ppy)$_2$(substituted 1,10-phen)][PF_6] (ppy = 2-phenylpyridine) and [Ir(pq)$_2$(substituted 1,10-phen)][PF_6] (pq = 2-phenylquinoline) complexes, a promising class of cationic Ir(III) complexes for electroluminescent devices. While the absorption and emission energies are slightly affected by substitution on the phenanthroline ligand, quantum yields and emission lifetimes are affected by significant changes. The highest quantum yields (Φ = 34−38%) are obtained with 5-methyl-1,10-

phenanthroline, while negligible values are obtained by substitution in position 5 of the methyl group with an electron-donor group such as NMe_2 ($\Phi = 0.3-6\%$) or an electron-withdrawing substituent such as NO_2 ($\Phi < 0.1\%$). The presence of two methyl groups or of two π-delocalized phenyl substituents on the phenanthroline ligand leads to lower quantum yields ($\Phi = 20-26\%$) but still higher than that of the reference complex bearing 1,10-phenanthroline ($\Phi = 7\%$). The investigated complexes display only a slight color tunability, with the emissions ranging from 534 to 592 nm, but an emissive lifetime ranging from 1.27 to 4.03 μs and from 0.19 to 0.82 μs under deaerated and non-deaerated conditions, respectively. Interestingly, the more sterically crowded complex **4** shows the lowest deaerated/not-deaerated lifetimes ratio, due to steric hindrance toward the interaction with triplet oxygen. Detailed theoretical calculations and electrochemical investigations show a nice correlation of the trend of the HOMOs and LUMOs energy levels of the complexes investigated. TDDFT calculations of the lowest singlet and triplet excited states at the singlet ground-state and triplet excited-state geometries have allowed us to assign the main bands of the absorption spectra to $\pi-\pi^*$ transitions centered on the π-delocalized ppy, pq, and phen ligands (higher energy) and to the MLCT with arriving states on the phenanthroline ligand (lower energy), with the emission band originating from a ^{3}MLCT excited state localized on the phenanthroline ligand.

Some general observations can be finally made, based upon our combined experimental and theoretical investigations:

(i) Weak electron-donating substituents like the methyl group do not significantly alter the geometry and the electronic structure of the Ir(III) cationic complexes investigated in this work; an exception is represented by complex **6** with two methyl groups in positions 2 and 9 of the phenanthroline ligand, for which steric hindrance to the metal coordination alters the metal-to-phenanthroline bond distances and consequently perturbs the electronic structure, as clearly evidenced also by the electrochemical investigation. The substitution of methyl groups by phenyl groups in positions 4 and 7 (e.g., complexes **3a** and **4**) does not perturb the electronic structure, in particular the pattern of the LUMO orbitals, although the LUMO/LUMO+1 and LUMO+1/LUMO+2 gaps are slightly affected.

(ii) Strong electron-withdrawing substituents, such as the NO_2 group, lead to extensive perturbation of the phenanthroline π^* levels, which is reflected in a strong LUMO stabilization. Strong electron-donor substituents, such as NMe_2, destabilize the π-bonding levels of the phenanthroline ligand, which shift quite close to the HOMO. This is clearly reflected by the more complex oxidation behavior observed in the electrochemical investigation of complexes **1b** and **2b**. In addition, the presence of a NMe_2 group leads not only to the destabilization of the HOMO but also to major effects on the LUMO/LUMO+1 and LUMO+1/LUMO+2 gaps as expected for a significant perturbation of both the π and π^* levels of the phenanthroline ligand.

(iii) Replacing the ancillary phenylpyridine ligand by phenylquinoline does not affect the nature and composition of the lowest excited states; the only effect is a stabilization of the phenylquinoline-based LUMO+2/LUMO+3, which eventually become almost isoenergetic with the phenanthroline-based LUMO/LUMO+1.

(iv) The overall quantum yields of complexes carrying methyl or phenyl substituents on the phenanthroline ligand are mainly controlled by nonradiative processes of decay, since rather limited variations of k_r are measured, as opposed to a wider k_{nr} variation range. The limited k_r variation is in agreement with the modest electronic-structure change observed for these complexes. The k_{nr} variability seems therefore not to be related to major changes of the electronic structure but rather to significant perturbation of the phenanthroline ring deformation motions either by the different nature of the substituents or by their positions on the phenanthroline ligand. However, the presence of a strong electron donor like NMe_2 or of a strong electron-withdrawing substituent produces a quenching of the quantum yield, which could be related partially to the significant perturbation of the electronic levels.

Overall, our work has shown that substitution on the phenanthroline ligand in cationic Ir(III) complexes of type $[Ir(ppy)_2(phen)]^+$ and $[Ir(pq)_2(phen)]^+$ does not influence the emission color very much but strongly influences quantum yields. Our work also provides evidence that the dominant role of the nonradiative pathway of decay is strongly dependent upon the nature and type of substitution.

Acknowledgment. We deeply thank Prof. Camilla Ferrante (Università di Padova) for fruitful discussions and Drs. Martina Bonacina, Li Cong, Francesco Morosini, and Matteo Parravicini for experimental help. This work was supported by the Ministero dell'Istruzione, dell'Università e della Ricerca (Programma di ricerca FIRB, year 2003; research title, Molecular compounds and hybrid nanostructured materials with resonant and non-resonant optical properties for photonic devices) and by CNR (PROMO 2006; research title, Sistemi molecolari e nanodimensionali con proprietà funzionali: Nanostrutture organiche, organometalliche, polimeriche ed ibride; ingegnerizzazione supramolecolare delle proprietà fotoniche e dispositivistica innovativa per optoelettronica).

Supporting Information Available: Energies of the frontier molecular orbitals and energy differences between some frontier molecular orbitals for complexes **1**−**7** in CH_3CN solution and in CH_2Cl_2; isodensity plots of selected molecular orbitals of **1b**−**d** and **2b** complexes; comparison between the experimental and computed UV−vis absorption spectra of **1a**, **1d**, **3a**, and **3b** complexes; cyclovoltammetric patterns of compounds **2a**−**c** and **4**−**6**; graph of E_{em} vs $\ln(k_{nr})$ for **1a**, **1d**, and **2a**; graph of the experimental vs the calculated HOMO−LUMO energy gaps. This material is available free of charge via the Internet at http://pubs.acs.org.

IC700414Z